

# Source Mechanisms of Earthquakes Near Mid-Ocean Ridges From Body Waveform Inversion: Implications for the Early Evolution of Oceanic Lithosphere

ERIC A. BERGMAN AND SEAN C. SOLOMON

*Department of Earth, Atmospheric, and Planetary Sciences, Massachusetts Institute of Technology, Cambridge*

To investigate the early tectonic evolution of oceanic lithosphere, we present a synthesis of the characteristics of near-ridge earthquakes, i.e., earthquakes which occur off the axis of major mid-ocean spreading centers but in lithosphere less than 35 m.y. old. Near-ridge seismicity for the past two decades has been rather evenly distributed along the major ridge systems, with the exception of the central Indian Ocean and the eastern part of the Cocos plate, which have experienced a high rate of earthquake activity during that time. For 32 near-ridge earthquakes we determined the double-couple orientation, seismic moment, centroid depth, and source time function, using a formal inversion technique based on matching synthetic and observed *P* and *SH* waveforms. All types of faulting styles are observed. Seismogenic deformation in young oceanic lithosphere is concentrated in the first 15 m.y., and occurs almost entirely in the uppermost mantle, from just below the Moho to depths at which the temperature estimated from standard thermal models exceeds 800°C. Thrust faulting is not observed at depths greater than 10 km below the seafloor. The deepest near-ridge earthquakes are generally characterized by normal-faulting focal mechanisms, with the *T* axis oblique or perpendicular to the local spreading direction; most of these earthquakes occur in the central Indian Ocean. The transition from mechanisms characteristic of ridge axes to those characteristic of the near-ridge environment occurs within the first few million years. For lithosphere less than 35 m.y. old, horizontal compressive stress associated with the cooling and subsidence of the lithosphere ("ridge push") does not appear to be the dominant source of stress released in earthquakes; this result may be used to place a lower bound of several hundred bars on the typical stress difference in young oceanic lithosphere. This bound, together with the observed depth of faulting, implies that the strain rate associated with seismic deformation is locally at least  $10^{-15} \text{ s}^{-1}$ . We propose that thermoelastic stresses associated with plate cooling play an important role in near-ridge earthquakes. This source of stress can account for the mechanisms and depths of many near-ridge earthquakes and for the concentration of activity in very young lithosphere. The comparative aseismicity of the oceanic crust may reflect the concentration of thermoelastic stress below the Moho due to different material properties for the crust and upper mantle or the early release of thermoelastic stresses through hydrothermal circulation and cracking throughout the crust at or near the ridge axis. The higher level of near-ridge seismicity in the Indian Ocean may be the result of modification or enhancement of the more typical near-ridge stress state by such local processes as the continental collision between India and Asia or active secondary convection beneath the young lithosphere of the Indian plate.

## INTRODUCTION

Source mechanism studies of earthquakes on the mid-ocean ridge system have played an important role in validating the plate tectonic hypothesis because the faulting mechanisms are thought to reflect directly the relative motions between plates [e.g., Sykes, 1967; Minster and Jordan, 1978]. Intraplate earthquakes have also been extensively studied because their mechanisms constrain the long-wavelength tectonic stress field which may provide insight into the distribution of forces driving plate motions [e.g., Sykes and Sbar, 1974; Richardson et al., 1979; Bergman and Solomon, 1980]. Earthquakes occurring in very young oceanic lithosphere, but off the ridge axis, resist easy classification as intraplate or plate boundary events in the usual sense and until recently have received less attention [Wiens and Stein, 1983b; Wiens et al., 1983; Bergman and Solomon, 1983; Bergman et al., 1984]. This paper presents an evaluation of the tectonics of the near-ridge environment based on the source mechanisms of earthquakes in young oceanic lithosphere.

The near-ridge tectonic environment is potentially influenced by a variety of processes. The most rapid evolution of

the thermal and mechanical state of oceanic lithosphere generally occurs during the first few tens of millions of years [e.g., Parsons and Sclater, 1977; Watts et al., 1980]. Complications to the simple conductive cooling of the lithosphere may arise both from hydrothermal convection in the oceanic crust [e.g., Lister, 1977; Fehn and Cathles, 1979] and from secondary convection in the asthenosphere [Parsons and McKenzie, 1978; Buck, 1984]. The consequent spatial and temporal variations in temperature are likely to be large enough to produce tectonically significant thermoelastic stresses, at least locally [Turcotte and Oxburgh, 1973; Turcotte, 1974]. During the first few tens of millions of years the large topographic relief of the median valley and flanking mountains along slow-spreading ridges is reduced, by presumably tectonic processes [e.g., Macdonald and Atwater, 1978; Tapponnier and Francheteau, 1978], and the area-integrated "ridge push" begins to have an appreciable effect on the state of stress [e.g., Lister, 1975; Dahlen, 1981]. Nonuniformity in the spreading process may produce localized stress concentrations. Stresses transmitted through the lithosphere from other plate boundaries may also be significant in some areas. Focal mechanisms and depths of earthquakes near ridges may be expected to reflect many of these processes and provide one of the more direct methods for studying their relative importance.

A thorough synthesis of the source mechanisms of near-ridge earthquakes provides a means as well for determining

Copyright 1984 by the American Geophysical Union.

Paper number 4B0952.  
0148-0227/84/004B-0952\$05.00

the nature and location of the transition between the ridge axis tectonic regime, characterized by horizontal extension perpendicular to the ridge axis [Sykes, 1967], and the stress regime in stable plate interiors, generally characterized by horizontal compression [Sykes and Sbar, 1974; Richardson *et al.*, 1979]. A better understanding of this transition facilitates the interpretation of other features of the intraplate stress field and provides a constraint on models of the interaction between the lithosphere and the upper mantle convective system [e.g., Stein and Wiens, 1983; Wiens and Stein, 1984]. Sykes and Sbar [1974] concluded on the basis of the limited data then available that this transition occurs at a lithospheric age of 10–20 m.y., and others [e.g., Fleitout and Froidevaux, 1983] have used this result as a major constraint in modeling the state of stress in oceanic lithosphere.

In order to address these issues, we have determined the source mechanism and focal depth of 32 near-ridge earthquakes, using a formal inversion technique based on matching synthetic and observed *P* and *SH* waves [Nabelek, 1984]. The source parameters of these earthquakes, together with other source mechanism data from the literature, allow a much more detailed examination than was previously possible of the deformation and causative processes accompanying the thermal and mechanical evolution of young oceanic lithosphere.

#### A CATALOG OF NEAR-RIDGE EARTHQUAKES

We began our study by assembling a list of near-ridge earthquakes which occurred since the establishment of the World-Wide Standard Seismograph Network (WWSSN) and which are large enough to study with body wave synthesis techniques. The search for such near-ridge earthquakes was based primarily on the catalog of the International Seismological Centre (ISC) for 1964–1979. All epicenters near the major mid-ocean ridge systems were plotted at a scale and projection which could be overlaid on maps of seafloor bathymetry. The locations of earthquakes with a body wave magnitude ( $m_b$ ) of at least 5.4 were noted and judged as to whether they were resolvable off the ridge axis. For the purposes of this study the near-ridge environment was taken to include oceanic lithosphere less than about 35 m.y. old. We have excluded earthquakes in back arc or marginal basins [e.g., Wang *et al.*, 1979], however, since such regions may not be representative of young oceanic lithosphere. The near-ridge earthquakes satisfying these criteria are listed in Table 1.

The approach taken here may introduce a bias in the representation of seismicity in the very youngest lithosphere, since the typical epicentral uncertainty (20–30 km) is such that we might have difficulty distinguishing between ridge axis earthquakes and earthquakes in very young (2–5 m.y. old) lithosphere along slow-spreading ridges. Source studies of ridge axis earthquakes along slow-spreading ridges, performed with the same body wave inversion technique as is used here, reveal several consistent features of such earthquakes which give added confidence that our catalog of near-ridge events is both relatively complete and uncontaminated by ridge axis events near slow-spreading ridges. Ridge axis events are found to be extremely shallow (centroid depth less than 3 km below the seafloor), located within the median valley (strongly constrained by the water depth inferred from the prominent reverberations in the water column observed on vertical component seismograms), and characterized by nearly pure normal faulting with nodal planes dipping at about 45° and striking parallel to the overall trend of the ridge axis [Tréhu *et al.*, 1981; Solomon *et al.*, 1983; Huang *et al.*, 1984; Jemsek *et al.*,

1984]. With perhaps one exception, none of these features are shared by any of the near-ridge earthquakes in Table 1. We are thus reasonably confident that our catalog provides an unbiased global view of larger earthquakes in oceanic lithosphere between the ages of a few and 35 m.y. over the last two decades.

Table 1 includes two events which occurred before 1964 and which have published mechanisms from *P* wave first motions [Sykes, 1967; Tobin and Sykes, 1968] and several events since 1980, primarily earthquakes from the catalogs of Dziewonski and Woodhouse [1983] and Dziewonski *et al.* [1983]. In addition, Table 1 includes several events with  $m_b < 5.4$  where there is some information about the source, either a published focal mechanism or a successful body wave inversion. The age listed for each event in Table 1 is determined either from published identifications of magnetic anomalies and the chronology of LaBrecque *et al.* [1977] or from the compilation of isochrons of Sclater *et al.* [1980]. The uncertainty in the listed age for each event is a function of location error, local spreading rate, and possible errors in the identification of magnetic anomalies; an uncertainty of 2 m.y. is regarded as typical. For the exceptions where an epicenter lies near a fracture zone with significant offset or in an area for which there is considerable uncertainty in the age, a range of possible ages is given in Table 1.

The global distribution of the 58 near-ridge earthquakes in Table 1 is shown in Figure 1. Except for the central Indian Ocean and a small area in the eastern Pacific, which are notably more active, near-ridge earthquakes are distributed rather evenly along the major mid-ocean spreading centers. This is in striking contrast to teleseismically observed ridge axis earthquakes: no such events have been observed on the fast-spreading East Pacific Rise, yet several dozen earthquakes with  $m_b \geq 5.4$  have been observed on the slow-spreading Mid-Atlantic Ridge. These variations cannot be attributed to different detection limits, since the ISC has nearly complete global detection capability for earthquakes with  $m_b > 5.2$  [Chinnery, 1978]. Thus there appears to be no correlation between the levels of near-ridge and ridge axis seismicity.

#### SOURCE PARAMETERS FROM BODY WAVEFORM INVERSION

For 32 of the earthquakes listed in Table 1 we determined the best fitting double-couple point source, using a formal inversion of the long-period *P* and *SH* waveforms [Nabelek, 1984]. The inversion procedure yields centroid depth and source time function as well as double-couple orientation and moment. The source mechanisms of nine of these earthquakes have been described in an earlier study [Bergman *et al.*, 1984], which also contains a more detailed discussion of the inversion procedure. Mechanisms of the remaining 23 events are discussed in the appendix.

All inversions were performed with the same source velocity structure: a water layer with depth estimated from bathymetric maps, a single crustal layer of thickness 6 km and seismic velocities  $V_p = 6.4$  km/s and  $V_s = 3.7$  km/s, and a mantle half space with  $V_p = 8.1$  km/s and  $V_s = 4.6$  km/s. The source depths in Table 1 are relative to the top of the crustal layer. Differences between the actual velocity structure in the epicentral regions and the model source structure are unlikely to be large enough to bias seriously the inversion results. For events at depths near the crust-mantle boundary, there is a potential for bias, as a result of using incorrect takeoff angles, in the inferred focal mechanism. The use of both *P* and *SH* waves, which have radically different radiation patterns, serves

TABLE 1. Epicentral Data, Source Parameters, and Lithospheric Age for Earthquakes in Young Oceanic Lithosphere

Date	Origin Time	Latitude °N	Longitude °E	$m_b$	$M_s$	$M_0^a$	Mechanism <sup>b</sup>	Depth <sup>c</sup>	Age, m.y.	Location
Aug. 6, 1962	0135:27.7	32.26	-41.03			13	288/43/315	10	8	North Atlantic Ridge
Aug. 22, 1963	0927:05.8	42.08	-126.19				143/90/180 <sup>d</sup>		3	Gorda Ridge
June 12, 1964	1644:35.6	2.19	-83.13	5.4					3	Cocos-Nazca Ridge
Sept. 17, 1964	1502:01.5	44.58	-31.34	5.5			222/68/130 <sup>e</sup>		20	North Atlantic Ridge
Sept. 9, 1965	1002:25.7	6.51	-84.44	5.8		24	173/88/160	8	12/18	Cocos Ridge
Sept. 12, 1965	2202:37.7	-6.46	70.76	6.1	6.0	33	263/44/246	18	16/32	Central Indian Ridge
Nov. 25, 1965	1050:50.8	-17.07	-100.24	5.3		1.8 <sup>f</sup>	022/46/110 <sup>f</sup>	9 <sup>f</sup>	20	Nazca plate
Dec. 19, 1965	2206:33.0	-32.24	78.87	5.5		13 <sup>g</sup>	300/68/304 <sup>g</sup>	11 <sup>g</sup>	4	Southeast Indian Ridge
Feb. 17, 1966	1147:57.3	-32.20	79.93	6.0		84 <sup>h</sup>	276/60/290 <sup>h</sup>	12 <sup>h</sup>	4	Southeast Indian Ridge
Feb. 17, 1966	1243:02.0	-32.15	79.04	5.6					4	Southeast Indian Ridge
March 28, 1966	0444:12.2	-32.12	78.84	5.5					4	Southeast Indian Ridge
Jan. 7, 1967	0027:23.0	-48.80	112.76	5.5		12	016/41/236	9	2.5	Southeast Indian Ridge
Nov. 10, 1967	1838:34	-6.03	71.34	5.2		3.0	234/76/191	18	20/36	Central Indian Ridge
Nov. 11, 1967	1155:56	-6.01	71.36	5.3	5.2	3.7	264/50/261	17	20/36	Central Indian Ridge
Nov. 11, 1967	1214:55.0	-6.03	71.34	5.6	5.8				20/36	Central Indian Ridge
Nov. 11, 1967	1759:57.0	-6.10	71.32	5.4					20/36	Central Indian Ridge
Nov. 21, 1967	1702:25.8	72.66	8.14	5.4					10	North Atlantic Ridge
Feb. 20, 1968	0219:49.5	12.40	-46.94	5.5			normal <sup>e</sup>		17	North Atlantic Ridge
March 2, 1968	2202:24.2	-6.09	71.41	5.5	5.4	7.7	284/52/280	13	20/36	Central Indian Ridge
Oct. 8, 1968	0743:22.8	-39.85	87.74	5.8	5.8	23 <sup>g</sup>	006/54/269 <sup>g</sup>	9 <sup>g</sup>	5	Southeast Indian Ridge
July 25, 1969	2130:33.3	12.44	-40.75	4.8			thrust <sup>e</sup>		20/35	North Atlantic Ridge
Aug. 8, 1969	1108:13.2	-47.76	-15.66	5.7		15	008/67/215	7	8/19	South Atlantic Ridge
Jan. 21, 1970	1751:37.4	7.03	-104.24	6.1	6.8	140	332/41/106	6	3	East Pacific Rise
March 31, 1970	1818:28.0	-3.78	69.70	5.5	5.5	8.0	043/83/187	13	12	Central Indian Ridge
April 25, 1970	0343:31	-6.29	69.84	5.1	5.1	1.6	248/85/192	11	13	Central Indian Ridge
May 9, 1971	0825:01.1	-39.78	-104.87	6.0	6.0	53	025/46/104	9	9	Pacific-Antarctic Ridge
May 9, 1971	1801:00.3	-39.77	-105.10	5.4					9	Pacific-Antarctic Ridge
May 2, 1972	0656:23.2	5.22	-100.32	5.9	5.5	18	332/49/280	11	3	East Pacific Rise
May 3, 1973	2311:04	-46.14	73.22	5.5	5.5	8.0 <sup>g</sup>	185/50/253 <sup>g</sup>	16 <sup>g</sup>	27	Southeast Indian Ridge
June 29, 1973	0755:12.7	3.93	-85.03	5.4	4.9	2.6	353/61/169	6	7/11	Cocos-Nazca Ridge
Nov. 17, 1973	1051:19.6	-1.59	69.85	5.4	5.5	4.8	046/51/226	20	12	Central Indian Ridge
Jan. 18, 1974	2114:51.2	-34.08	-20.15	5.4					22/25	South Atlantic Ridge
July 1, 1974	2311:14.5	-22.57	-10.68	5.5	5.5	3.3	068/29/092	3	9	South Atlantic Ridge
Sept. 11, 1975	2200:01.3	7.05	-104.18	6.3	5.8	11	307/44/093	5	3	East Pacific Rise
Sept. 19, 1975	0337:11	-34.74	81.88	5.9	6.1	49 <sup>g</sup>	241/63/275 <sup>g</sup>	18 <sup>g</sup>	13	Southeast Indian Ridge
Oct. 29, 1975	0501:49	4.07	-103.51	5.4			normal <sup>h</sup>		2.5	East Pacific Rise
March 29, 1976	0539:36.3	3.96	-85.88	5.8	6.5	92	199/82/181	8	11	Cocos-Nazca Ridge
Aug. 4, 1976	1400:01.6	-35.62	-14.02	5.7	5.4				5/17	South Atlantic Ridge
Oct. 21, 1976	0356:28.1	-57.37	-161.07	5.4					21	Pacific-Antarctic Ridge
Nov. 2, 1976	0713:17	-29.36	77.65	5.8		76 <sup>g</sup>	231/37/282 <sup>g</sup>	14 <sup>g</sup>	9	Southeast Indian Ridge
Nov. 2, 1976	1119:15	-29.24	77.79	5.6		5.6 <sup>g</sup>	249/41/293 <sup>g</sup>	14 <sup>g</sup>	10	Southeast Indian Ridge
Feb. 17, 1977	2025:21.5	-45.39	-19.06	5.4	5.2				14/18	South Atlantic Ridge
April 11, 1977	0215:18.4	-52.24	114.66	5.4	5.4				5	South of Australia
Aug. 26, 1977	1950:02.3	-59.54	-20.59	6.3	7.1	540	091/85/175	9	10/17	American-Antarctic Ridge
Dec. 14, 1977	0300:14.0	-33.84	57.98	5.5	5.1	2.8	018/51/288	6	27	Southwest Indian Ridge
Jan. 5, 1978	0323:26.2	-20.79	-126.95	5.5					23	East Pacific Rise
April 3, 1978	0609:36.6	-52.21	114.61	5.4					5	Southeast Indian Ridge
May 22, 1979	0155:55.8	-43.81	79.00	5.5	5.1	3.6 <sup>g</sup>	197/49/280 <sup>g</sup>	17 <sup>g</sup>	9	Southeast Indian Ridge
Dec. 13, 1979	0243:36.9	5.55	-80.48	5.4	5.5	8.7	349/75/178	13	21	Panama Basin
March 6, 1981	1943:00.3	3.93	-85.88	5.9	6.5				11	Cocos-Nazca Ridge
Sept. 13, 1981	0919:30.9	24.87	-46.30	5.8	5.5	8.9	021/33/264	11	4.5	North Atlantic Ridge
Sept. 24, 1981	2109:42.6	-45.65	79.86	5.4	5.5	4.4 <sup>g</sup>	142/37/247 <sup>g</sup>	11 <sup>g</sup>	14	Southeast Indian Ridge
Sept. 30, 1981	2303:54.4	-5.09	-111.98	5.9	5.2	2.2 <sup>i</sup>	270/47/054 <sup>i</sup>		6/15	East Pacific Rise
Dec. 12, 1981	2331:10.9	4.89	70.15	5.5	5.1	2.3	060/50/307	15	35	Carlsberg Ridge
April 10, 1982	0647:54.3	-34.33	58.33	5.6	5.4	2.5 <sup>j</sup>	133/36/319 <sup>j</sup>		32/38	Southwest Indian Ridge
April 18, 1982	1131:04.3	-29.07	-113.84	5.9	5.8	14 <sup>j</sup>	140/43/085 <sup>j</sup>		3	East Pacific Rise
June 8, 1982	0304:05.5	-34.03	58.39	5.5					32/38	Southwest Indian Ridge
Sept. 8, 1982	2112:31.5	-34.50	58.29	5.4	5.2	2.6 <sup>j</sup>	335/42/341 <sup>j</sup>		32/38	Southwest Indian Ridge

Epicentral data and magnitudes are from ISC (1964–1981) and National Earthquake Information Service (NEIS) (1982). Except where noted, all source parameters ( $M_0$ , depth, mechanism) have been determined in this study.

<sup>a</sup>Seismic moment in units of  $10^{24}$  dyn cm ( $10^{17}$  N m).

<sup>b</sup>Focal mechanism (strike, dip, slip, all in degrees) specified with the convention of *Aki and Richards* [1980].

<sup>c</sup>Depth in kilometers relative to the seafloor.

<sup>d</sup>*Tobin and Sykes* [1968].

<sup>e</sup>*Sykes and Sbar* [1974].

<sup>f</sup>*Mendiguren* [1971].

<sup>g</sup>*Bergman et al.* [1984].

<sup>h</sup>D. A. Wiens (personal communication, 1983).

<sup>i</sup>*Dziewonski and Woodhouse* [1983].

<sup>j</sup>*Dziewonski et al.* [1983].

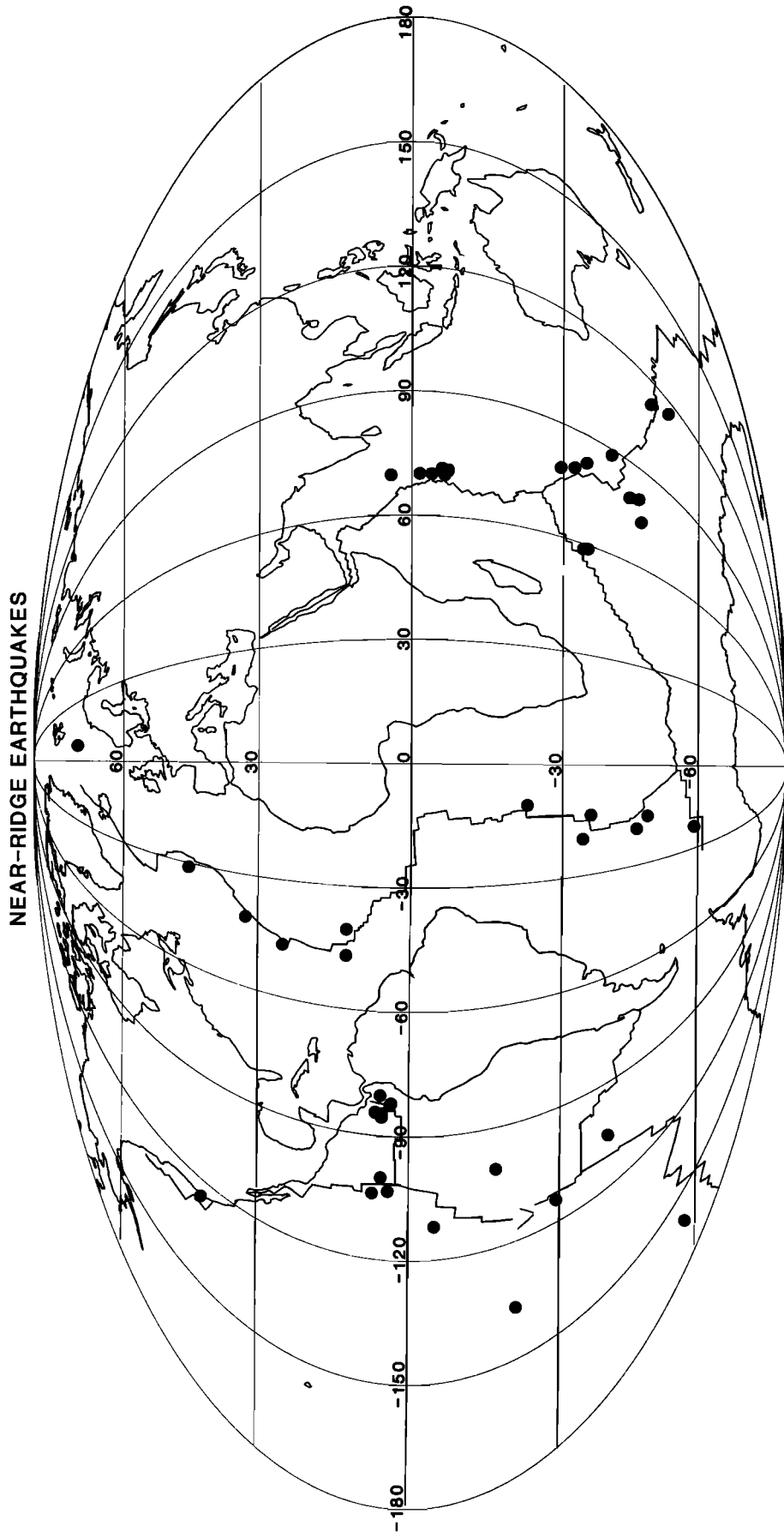


Fig. 1. Epicentral locations of the 58 near-ridge earthquakes listed in Table 1. Coastlines and oceanic spreading centers are also shown. Mollweide projection.

to minimize this problem, as does good azimuthal coverage.

Because the mechanical properties of the oceanic lithosphere depend strongly on depth as well as age, source depth is an extremely important source parameter. The formal error ( $2\sigma$ ) in the centroid depth calculated in the body wave inversion generally ranges between 0.6 and 1.0 km, but because the dependence of the waveforms on depth is highly nonlinear, this estimate of the resolution may be substantially biased [Tarantola and Valette, 1982]. The depth estimated in the inversion is also very sensitive to the alignment in time of the synthetic and observed waveforms; the formal depth resolution does not reflect this source of error. We estimate the average depth resolution of the body waveform inversion method to be about 2 km for the events studied here. It should be noted that because the body wave inversion yields the centroid depth of the best fitting point source rather than the depth at which rupture initiated, the maximum depth of seismic failure will always be greater than the centroid depth by an amount which depends on unknown features of the fault geometry and rupture process. Aside from the 32 events for which source parameters were determined in this study, the only other well-resolved source depth published for a near-ridge earthquake is for an event in the Nazca plate [Mendiguen, 1971] that was too small and too remote to permit an inversion of the long-period body waveforms.

Focal mechanisms, based primarily on short-period  $P$  wave first motions, have been published for several near-ridge earthquakes which we were unable to investigate by long-period body waveform inversion; these mechanisms are indicated in Table 1. We have also listed in Table 1 the seismic moments and focal mechanisms determined by Dziewonski and Woodhouse [1983] and Dziewonski et al. [1983] for four of the most recent near-ridge events by means of a semiautomated inversion of waveform data from the Global Digital Seismic Network. The long-period passband of the data used in their technique precludes good resolution of the centroid depth for very shallow events, however.

#### SOURCE PARAMETER-AGE RELATIONS

The deformation represented by near-ridge earthquakes is strongly influenced by the mechanical properties of young oceanic lithosphere and is thus likely to be a strong function of both depth and lithosphere age [Chen and Molnar, 1983; Wiens and Stein, 1983a]. The well-determined centroid depths of near-ridge earthquakes, distinguished on the basis of the ocean in which they occurred, are shown as a function of lithosphere age in Figure 2. As noted above (Figure 1), an unusually large number of near-ridge earthquakes have occurred in the Indian Ocean. Figure 2 also demonstrates that the Indian Ocean accounts for most of the near-ridge seismicity at focal depths in excess of 10 km. The deeper earthquakes in the Indian Ocean and one event each near the East Pacific Rise and the Mid-Atlantic Ridge occur at depths where standard plate-cooling models [Parsons and Sclater, 1977] predict a temperature of approximately 800°C. In contrast, few earthquakes in older oceanic lithosphere are found to occur at depths corresponding to such a high temperature [Chen and Molnar, 1983; Wiens and Stein, 1983a; Bergman, 1984].

Nearly all of the earthquakes included in this study have centroid depths in excess of 5 km. In normal oceanic lithosphere the Moho is found at a depth of about 6 km [e.g., Ewing and Houtz, 1979]. The data of Figure 2 suggest that earthquake faulting in young oceanic lithosphere occurs mostly in the uppermost mantle, immediately below the

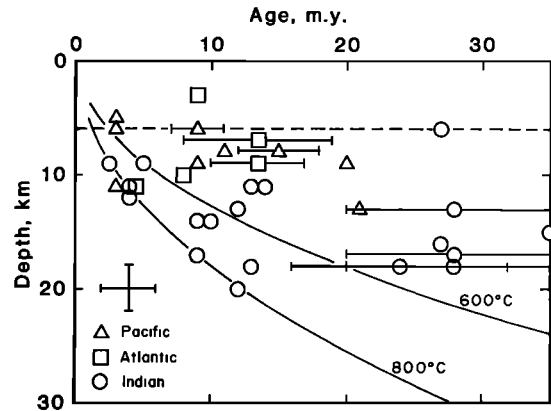


Fig. 2. Centroid depth versus lithosphere age for near-ridge earthquakes occurring in the Atlantic, Pacific, and Indian oceans. All depths are relative to the seafloor. The horizontal dashed line indicates the depth of the Moho (6 km) in the velocity model used for the body waveform inversions. Representative uncertainties in depth ( $\pm 2$  km) and age ( $\pm 2$  m.y.) are indicated by the error bars in the lower left corner. The larger error bars on age for some events correspond to the range in age given in Table 1. The 600° and 800°C isotherms, calculated from the plate-cooling model of Parsons and Sclater [1977], are also shown.

Moho. The larger earthquakes, however, almost certainly rupture through the lower crust.

Another feature of near-ridge seismicity evident from Figure 2 is that the number of earthquakes is greater in the age range 0–15 m.y. than in the range 15–35 m.y. The decline in seismic activity is even more pronounced if the seismic moments ( $M_0$ ) of the earthquakes are considered. In Figure 3 the 33 earthquakes with well-determined centroid depths are divided into three categories: those with  $10^{24} \leq M_0 < 10^{25}$ , those with  $10^{25} \leq M_0 < 10^{26}$ , and those with  $M_0 \geq 10^{26}$ , where  $M_0$  is given in dyne centimeters ( $10^{-7}$  N m). One of the two earthquakes with  $M_0 > 10^{26}$  dyn cm (January 21, 1970) occurred in lithosphere with an age of about 3 m.y., and nearly all the earthquakes with  $M_0 > 10^{25}$  dyn cm occurred in lithosphere 15 m.y. in age or younger. (The apparent scarcity of smaller events in lithosphere younger than 10 m.y. is probably not a real effect, since Table 1 includes several such earthquakes for which we were unable to obtain source parameters through long-period body wave inversion.) We interpret these data as indicating that deformation accompanying the thermal and

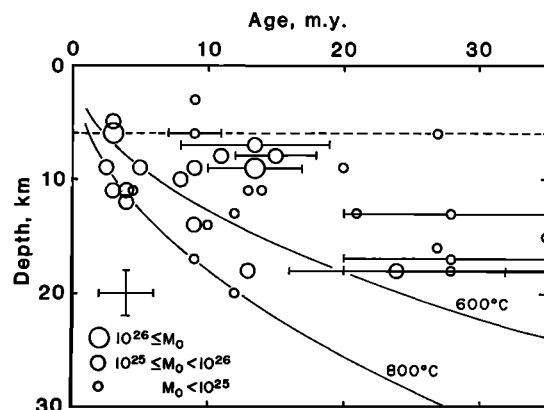


Fig. 3. Centroid depth versus lithosphere age for near-ridge earthquakes distinguished on the basis of seismic moment. All moments are in dyne centimeters. See Figure 2 for further explanation.

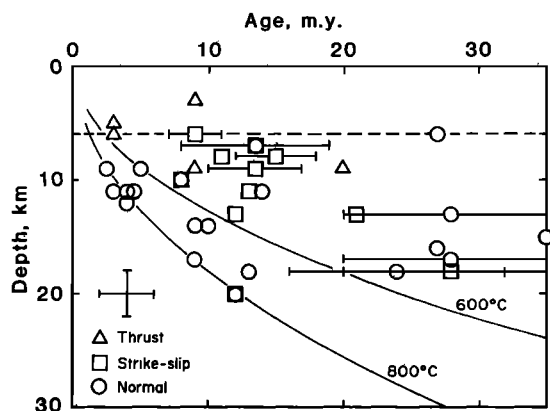


Fig. 4. Centroid depth versus lithosphere age for near-ridge earthquakes distinguished on the basis of whether the focal mechanism is characterized by thrust, strike-slip, or normal faulting. Where a focal mechanism is a combination of two of the basic faulting types, both symbols are superposed. See Figure 2 for further explanation.

mechanical evolution of young oceanic lithosphere is largely accomplished in the first 15–20 m.y.

Several interesting features of near-ridge tectonics emerge when the near-ridge earthquakes with known centroid depths are distinguished on the basis of focal mechanism type (Figure 4). In contrast to the mechanisms of earthquakes along ridge axes, focal mechanisms of normal-faulting near-ridge earthquakes frequently have significant strike-slip components and generally have  $T$  axes which are oblique or perpendicular to the local spreading direction. The only exception among the events we studied is the earthquake of September 13, 1981. Even this event differs from ridge axis events in having one steeply dipping nodal plane and a centroid depth of 11 km.

Near-ridge earthquakes characterized by strike-slip faulting are similarly distinct from transform fault earthquakes. In every case (see the appendix), one nodal plane is subparallel to the local trend of fracture zones. While a number of near-ridge events with strike-slip mechanisms are located on or near fracture zones, the sense of motion is nearly always the same as the offset of the local ridge axis segments, opposite to that of a transform fault earthquake.

A distinct stratification of fault type is evident in Figure 4. Thrust faulting is confined to shallow depths (<10 km), while most of the deepest events at all ages are characterized by normal faulting; strike-slip faulting tends to occur at intermediate depths. There also seems to be a regional bias to fault type. Considering the 33 events with known depths, 15 of the 19 events in the Indian Ocean represent normal faulting, and only four events with large components of normal faulting are found outside the Indian Ocean. Four of the five thrust-faulting events occur in the Pacific Ocean, and none occur in the Indian Ocean. Strike-slip faulting occurs in all three oceans. The implications of these characteristics for the tectonic evolution of young oceanic lithosphere are discussed in the following sections.

#### NEAR-RIDGE SEISMICITY OF THE INDIAN OCEAN

A clear conclusion from our brief survey of near-ridge seismicity is that the Indian Ocean is distinctive in at least several respects: it accounts for a disproportionate share of global near-ridge seismicity; the near-ridge earthquakes in the Indian Ocean are found to be deeper than most events in the Pacific or Atlantic oceans at comparable age; and the Indian Ocean

near-ridge earthquakes have dominantly normal-faulting mechanisms. There are several ways to interpret these observations. One view is that the Indian Ocean events are fully representative of near-ridge tectonics and that only the limited span of observations has prevented the detection of comparable behavior near other ridge systems. An opposite interpretation is that the tectonic processes responsible for the Indian Ocean events are unique to the region, and thus the mechanisms of these earthquakes are not relevant to the general question of the evolution of young oceanic lithosphere.

We favor an intermediate interpretation: the near-ridge earthquakes of the Indian Ocean are at least partly the product of processes common to all young oceanic lithosphere, but the stress field near some portions of the Indian Ocean ridge system has been enhanced or modified by processes peculiar to the region. One piece of evidence in support of this view is that comparatively deep normal-faulting events in young oceanic lithosphere occur in regions other than the Indian Ocean (e.g., the May 2, 1972, and September 13, 1981, events).

For nine of the Indian Ocean events (Figure 5), located along the Southeast Indian Ridge (SEIR) and studied in detail by Bergman *et al.* [1984], the perturbing physical process has been tentatively identified. Three of the earthquakes, clustered in a small region of the Antarctic plate between the Kerguelen Plateau and the SEIR, are attributed [Bergman *et al.*, 1984] to thermal and bending stresses associated with a residual depth anomaly in the vicinity of a proposed horizontal "pipeline" for flow of asthenospheric material from the Kerguelen hotspot to the Amsterdam and St. Paul Islands region of the SEIR [Morgan, 1978]. The remaining six earthquakes, located at four sites spaced along a considerable length of the SEIR on the Indian plate, are speculatively attributed to the response of the Indian plate (and its associated upper mantle convective pattern) to the ongoing collision between the Indian and Asian plates [Bergman *et al.*, 1984].

Stein [1978] found focal mechanisms of the same type (normal faulting with  $T$  axis oblique to the local spreading direction) for several earthquakes comprising a swarm on the Chagos Bank, in young oceanic lithosphere of the Indian plate, near the Central Indian Ridge (CIR). We performed body waveform inversions for three of the Chagos Bank events studied by Stein [1978], confirming the basic source parameters (see the appendix). We also inverted the waveforms from four other near-ridge events in the same area, including one member of the Chagos Bank swarm not studied by Stein (November 10, 1967). The source mechanisms of these latter events reveal an aspect of the deformation of the lithosphere in this area not previously noted: three of the earthquakes, including the November 10, 1967, event, have right-lateral strike-slip mechanisms on planes striking northeast, parallel to the many fracture zones offsetting the CIR. The focal mechanism of the fourth earthquake (November 17, 1973) is a combination of the strike-slip and normal-faulting mechanisms observed in the area. The focal mechanisms of all the events near the CIR are shown in Figure 6.

Clearly, the deformation represented by the seismicity near the CIR is not an exact analog of the SEIR situation, since no strike-slip faulting has been observed in the latter region. The observation of a component of right-lateral shear along with the extensional deformation near the CIR, however, still permits the hypothesis that the near-ridge seismicity in both areas to some degree reflects plate-wide consequences of the continental collision. The geometry of the mid-ocean ridge system varies considerably between the SEIR and CIR, and horizon-

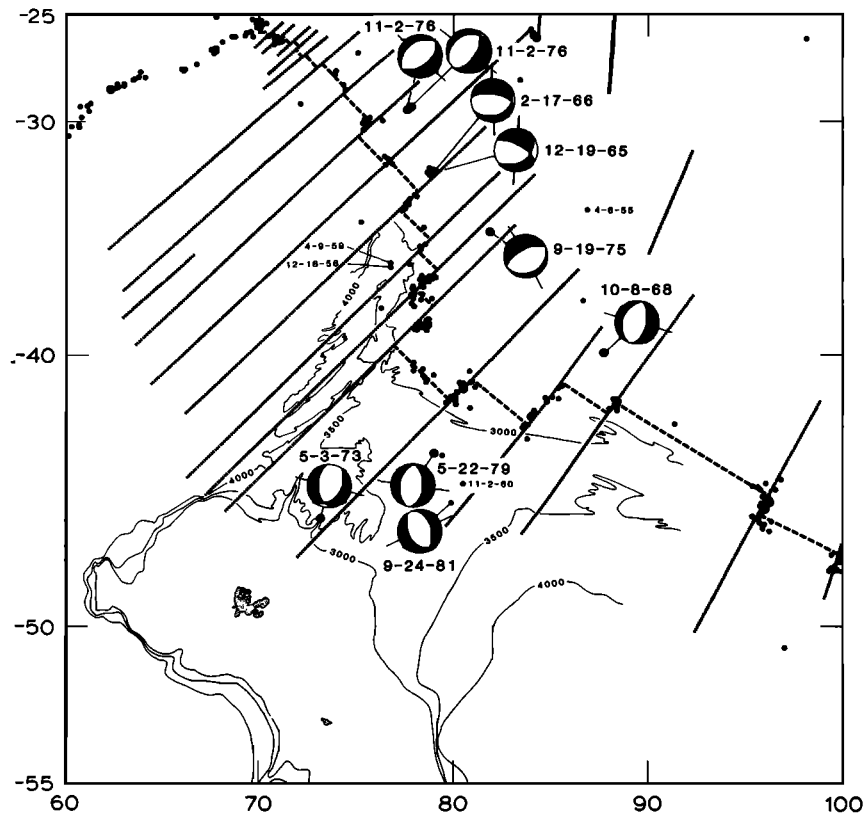


Fig. 5. Basic tectonic elements of the western part of the Southeast Indian Ridge, with locations and focal mechanisms of nine near-ridge earthquakes [Bergman *et al.*, 1984]. Tectonic elements from Schlich [1982]; ridge axis segments are shown as heavy dashed lines and fracture zones (defined by offsets in identified magnetic anomalies) as lighter dashed lines. Earthquake epicenters, shown as dots, are from Sykes [1970b] (1950–1964), ISC (1964–1979), and NEIS (1980–1982). Larger symbols indicate earthquakes with  $m_b \geq 5.5$ . Bathymetric contours [Hayes and Vogel, 1981; Fisher *et al.*, 1982] between the Kerguelen Plateau and the Southeast Indian Ridge indicate the region of the positive residual depth anomaly discussed by Bergman *et al.* [1984]

tally transmitted stresses in the lithosphere may be expected to vary as well. All focal mechanisms near the CIR are consistent with a lithospheric stress field in which the least compressive principal stress is horizontal and oriented approximately N-S.

The remaining near-ridge seismicity in the Indian Ocean consists of four events in a tight cluster on the Antarctic side of the Southwest Indian Ridge (SWIR) and several events along a short section of the SEIR south of Australia (Figure 1). All these earthquakes are quite small; we were able to perform waveform inversions for only one event in each location (January 7, 1967, and December 14, 1977). Both earthquakes are characterized by normal faulting with a significant component of strike-slip motion. Dziewonski *et al.* [1983] obtained focal mechanisms for two other events near the SWIR; the mechanisms are rather different from each other and from that of the event studied by us. The seismic activity at this site has been unusually high but appears to be limited to a small region.

#### DEEP NORMAL FAULTING IN YOUNG OCEANIC LITHOSPHERE

Normal-faulting earthquakes occur in young lithosphere in all oceans and constitute most of the deeper events at any lithosphere age between 3 and 35 m.y. (Figure 4). Whether or not the Indian Ocean is truly anomalous with respect to the processes producing the large number of normal-faulting earthquakes observed there, the depth distribution of such events has important implications for the mechanical and

thermal structure of young oceanic lithosphere and for the sources of lithospheric stress near mid-ocean ridges. We consider some of these implications in this section.

Of particular interest are those normal-faulting earthquakes which occur at depths within the oceanic lithosphere at which the temperature according to standard plate-cooling models [Parsons and Sclater, 1977] is approximately 800°C, so that ductile flow is expected to reduce the ability of the lithosphere to sustain significant differential stresses at an appropriate strain rate. To infer the nature and cause of the deformation represented by these deep normal-faulting earthquakes, estimates of the strength of the lithosphere as a function of temperature (i.e., depth) are necessary.

Strength envelopes for the lithosphere, giving the maximum sustainable differential stress as a function of depth, are now commonly encountered in the geophysical literature [e.g., Goetze and Evans, 1979; Brace and Kohlstedt, 1980; Meissner and Strehlau, 1982]. They all feature a near-surface strength which increases linearly with confining pressure according to a brittle failure law, typically that of Byerlee [1978]. The slope of this part of the strength envelope is a strong function of the assumed pore pressure; zero strength is predicted if pore pressure equals lithostatic pressure. The maximum strength occurs at the brittle-ductile transition, below which thermally activated ductile flow rapidly reduces with depth the differential stress which may be sustained. For a given geotherm the ductile flow law is primarily controlled by the assumed strain rate,

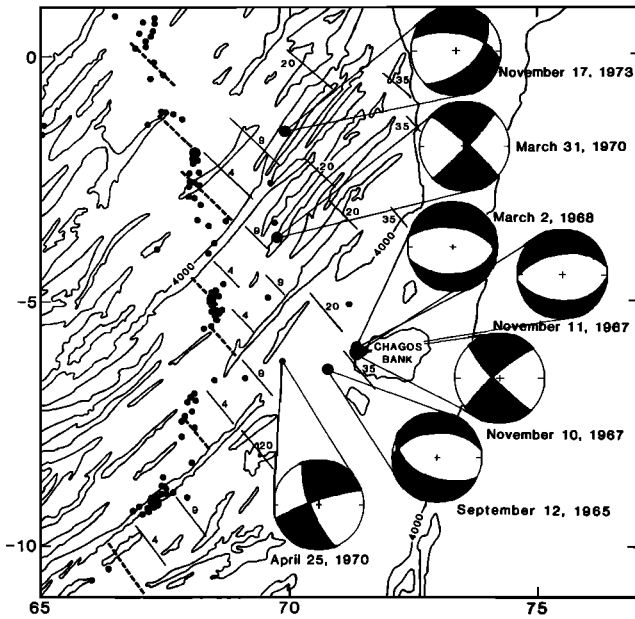


Fig. 6. Bathymetry, seismicity, and isochrons between the Central Indian Ridge and the Chagos Bank. The bathymetry of the region is represented by the 4000-m contour [from *Laughton, 1975; Fisher et al., 1982*]. The Chagos Bank is outlined by the 200-m contour. Focal mechanisms of near-ridge earthquakes determined in this study are shown. Solid dots indicate epicenters from the ISC (1964–1979), located from reported arrival times at 10 or more stations. Large dots indicate events with  $m_b \geq 5.4$ . The heavy dashed line indicates the position of the ridge axis. Isochrons (4, 9, 20, and 35 m.y.) are from the compilation of *Sclater et al. [1980]*.

with a higher strain rate allowing greater differential stress to be maintained at greater depths. The depth of the brittle-ductile transition is increased and the maximum sustainable differential stress is lowered with an increase in the pore pressure. A higher strain rate increases both the depth of the brittle-ductile transition and the maximum sustainable stress difference. Figure 7 illustrates these relationships for 15-m.y.-old lithosphere.

There are several potential sources of error in constructing that part of the strength envelope controlled by ductile flow. One is the selection of an appropriate rheology (e.g., “wet” versus “dry” olivine flow laws); another results from the extrapolation over many orders of magnitude from the strain rates achievable in the laboratory to those appropriate for tectonic problems. These strength envelopes obviously depend also on the accuracy of the geotherm, since the ductile flow laws are highly temperature-dependent. Hydrothermal circulation in the crust is thought to remove some fraction of the heat in young oceanic lithosphere [*Lister, 1977; Fehn and Cathles, 1979*], but little is known about the extent to which this circulation perturbs the geotherm in young oceanic lithosphere. The agreement between the observed seafloor depth-age relation and the subsidence curve calculated from the simple plate-cooling model [*Parsons and Sclater, 1977*] suggests that this model provides a good approximation to the average thermal state of at least the mantle portion of the oceanic lithosphere. Local departures from this model are certainly a possibility, however.

If earthquakes occur only at depths at which the strength envelope is controlled by the brittle failure law, high pore pressures (approaching the lithostat) and relatively low differential stresses must exist in the source regions of several of the

deepest normal-faulting earthquakes. The events in Figure 4 at about 4 m.y. age and 11–12 km depth fall into this category. *Kirby [1980]* has argued that pore pressure in the oceanic upper mantle is near zero, but we consider the question open, given the near absence of evidence. Near-lithostatic pore pressure is not required, however, if earthquakes can occur at depths below the brittle-ductile transition, where the ductile flow law still allows significant differential stress to be maintained. By this view, either brittle failure may occur at lower differential stress than predicted by Byerlee’s law or some earthquakes may represent rapid ductile failure. The source time functions inferred for the deepest normal-faulting earthquakes, however, are identical in character to those of shallower events. We take this as evidence that all of these earthquakes are the result of a single rupture process, most likely brittle failure.

If we assume that the deepest normal-faulting events define the depth at which lithospheric strength is reduced by ductile flow to a level insufficient for seismic failure, a joint constraint may be placed on the differential stress at which failure occurred and the corresponding strain rate of the deformation leading to seismic failure. If a minimum differential stress level is specified, a lower bound on the strain rate is implied. In Figure 8, curves defining the depth at which a representative range of stress levels are reached with the ductile flow law for dry olivine [*Goetze and Evans, 1979*] are shown for strain rates of  $10^{-13}$  and  $10^{-15} \text{ s}^{-1}$ . In order for a strain rate as low as  $10^{-15} \text{ s}^{-1}$  to be accommodated, the stress level associated with the deepest events can be no greater than a few hundred bars. A stress level in the kilobar range requires a strain rate of about  $10^{-13} \text{ s}^{-1}$ .

*Wiens and Stein [1983a]* estimated a strain rate of  $10^{-15} \text{ s}^{-1}$  for the seismically active Ninetyeast Ridge area of the Indian Ocean. If this strain rate were applicable to near-ridge deformation, a relatively low level of stress in young oceanic lithosphere would be implied. An average strain rate estimated from the seismic moments of a small number of earthquakes distributed over a broad region will always tend to be a lower

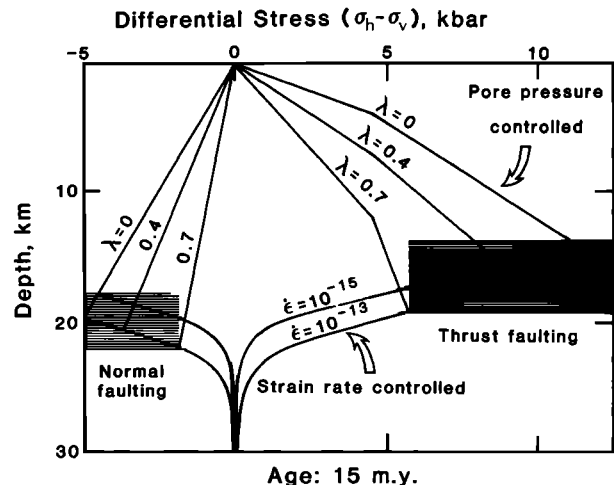


Fig. 7. Strength envelope for 15-m.y.-old lithosphere;  $\sigma_v$  and  $\sigma_h$  are the vertical principal stress and the horizontal principal stress with the largest absolute magnitude, respectively. Geotherm calculated from the model of *Parsons and Sclater [1977]*. The brittle failure law is from *Byerlee [1978]*, shown for several different values of the ratio  $\lambda$  of pore pressure to lithostatic pressure. The ductile flow law is for dry olivine [*Goetze and Evans, 1979*], shown at two values of strain rate  $\dot{\epsilon}$ . The hatched regions indicate the depth range through which the brittle-ductile transition may be moved by making different assumptions concerning the strain rate and pore pressure.

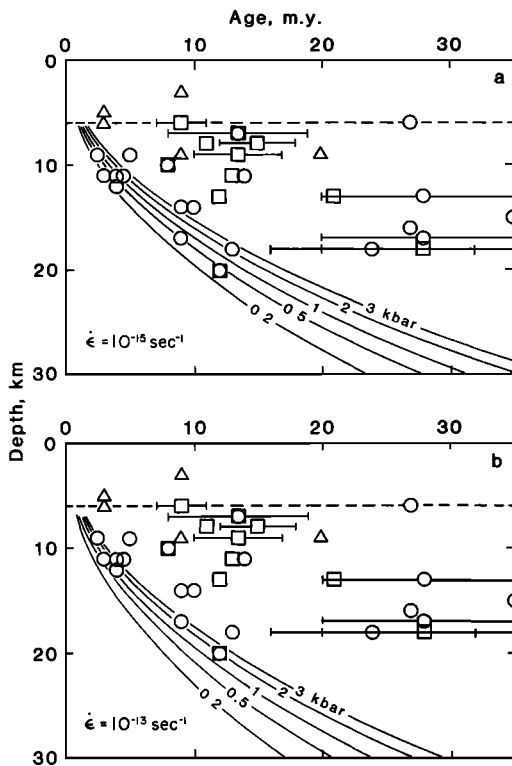


Fig. 8. Depth above which the ductile flow law yields differential stresses in excess of the indicated values (0.2, 0.5, 1.0, 2.0, and 3.0 kbar) for strain rates  $\dot{\epsilon}$  of (a)  $10^{-15}$  and (b)  $10^{-13}$  s $^{-1}$ . Near-ridge earthquakes are plotted as in Figure 4.

bound, however, given the possibility that oceanic intraplate deformation is concentrated near zones of significant strength variation, as is commonly observed in continental lithosphere [Sykes, 1978]. Strain rates as high as  $10^{-13}$  s $^{-1}$  have been inferred from naturally deformed rocks [e.g., Pfiffner and Ramsay, 1982]. In a later section we will argue that a minimum differential stress of several hundred bars is indicated by the lack of a clear influence of "ridge push" stress on the focal mechanisms of near-ridge earthquakes. In such a case, the characteristic strain rate of the deformation represented by near-ridge earthquakes is expected to be at least  $10^{-15}$  s $^{-1}$ .

#### THERMOELASTIC STRESS AND NEAR-RIDGE EARTHQUAKES

An important question concerns the source of the stress which gives rise to normal-faulting earthquakes in young oceanic lithosphere. We note that normal faulting characterizes most of the near-ridge earthquakes (with known depths and mechanisms) at depths below 10 km (Figure 4). Thermoelastic stresses resulting from the cooling of the lithosphere can account both for the observation of normal faulting at depth and the fact that the  $T$  axes of the focal mechanisms tend to be subparallel to the ridge axis [Turcotte and Oxburgh, 1973; Turcotte, 1974]. Bergman et al. [1984] discounted this mechanism as the primary cause of the earthquakes along the SEIR on the grounds that so little similar activity had been reported in other near-ridge areas. While the intraplate seismicity in the Indian Ocean is clearly more intense (at least over the last 20 years) than in most other areas, the results of this study show that normal-faulting near-ridge events are not confined to the central Indian Ocean. We consider here the implications of the assumption that thermoelastic cooling stresses are typical of all near-ridge environ-

ments but have been enhanced or modified in some manner at sites of anomalous near-ridge seismicity in the Indian Ocean.

The largest rate of release of thermoelastic stress in the cooling lithosphere is likely to be found near the region experiencing the highest differential cooling rate. The cooling rate as a function of age and depth in the plate-cooling model of Parsons and Sclater [1977] may be found analytically [e.g., Carslaw and Jaeger, 1959]. In Figure 9 are plotted contours of equal cooling rate as well as the curve defining the depth of the maximum cooling rate as a function of lithosphere age. At shallow depths near the ridge, very high cooling rates ( $>100^{\circ}$ /m.y.) are predicted, but hydrothermal circulation in the crust probably modifies significantly the shallow geotherm in this region, and much of the thermoelastic stress is likely to be relieved by shallow cracking within instantaneous volumes too small to result in a significant earthquake [e.g., Lister, 1977]. By 30 m.y., the upper 30 km of the oceanic lithosphere cools at a rate of  $10^{\circ}$ /m.y. or less. To an age of about 15 m.y., the deepest normal-faulting earthquakes parallel at a somewhat shallower depth the contour of maximum cooling rate. The concentration of near-ridge seismicity in lithosphere less than about 15 m.y. old supports the hypothesis of an important role for thermoelastic stresses, particularly since the vertical gradient of cooling rate is relatively high in this age range. Significant thermoelastic stresses can be expected in regions where the cooling rate varies rapidly with distance. A natural explanation for the cessation of seismicity at depths shallower than the depth of the maximum cooling rate is that the strength of the lithosphere at greater depths is too low for significant strain to accumulate.

Thermoelastic stresses related to plate cooling may also account for some instances of shallow thrust faulting in young oceanic lithosphere. The thermal stress in an elastic body is proportional to the product of  $\alpha E$  of the coefficient of thermal expansion and Young's modulus. Turcotte [1974] noted that for the oceanic crust,  $\alpha E$  may well be different from that of the upper mantle, so that the oceanic lithosphere reacts to temperature changes like a bimetallic strip. Using available (but not well constrained) material constants, Turcotte found that  $(\alpha E)_{\text{crust}} < (\alpha E)_{\text{mantle}}$ ; in which case, plate cooling produces higher thermal stresses in the upper mantle than the crust, a result consistent with the observation that near-ridge seismicity is concentrated below the Moho (Figure 3). The bimetallic strip analog, however, predicts thrust faulting only in the

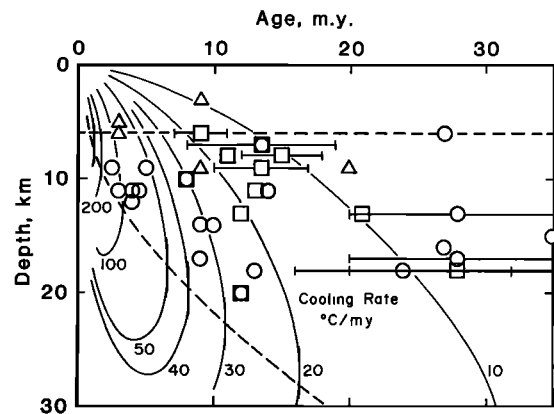


Fig. 9. Contours of equal cooling rate, calculated from the model of Parsons and Sclater [1977]. The dashed line traces the depth at which the cooling rate is a maximum as a function of age. Near-ridge earthquakes are plotted as in Figure 4.

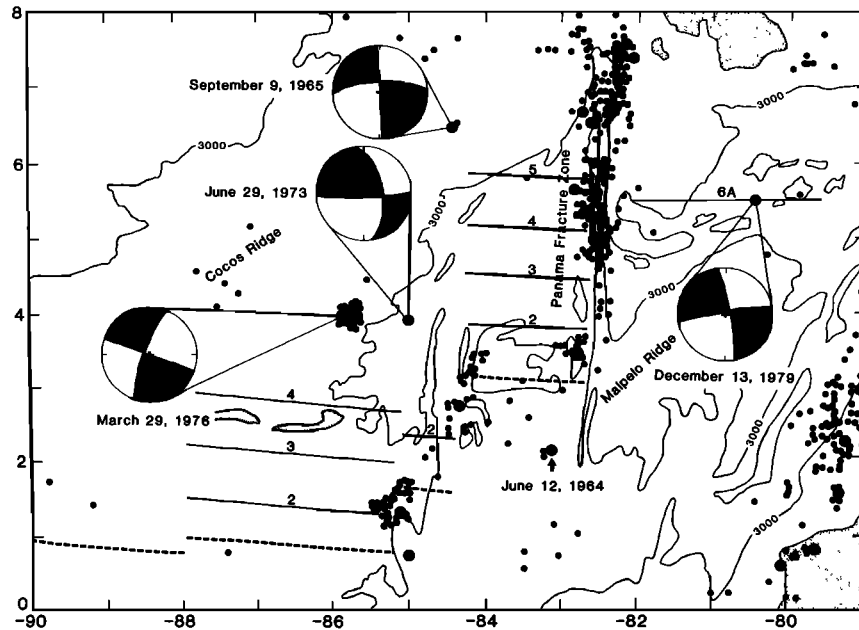


Fig. 10. Bathymetry, seismicity, and identified magnetic lineations in the epicentral region of the September 9, 1965; June 29, 1973; March 29, 1976; and December 13, 1979, earthquakes in the eastern Pacific. The epicenter of the June 12, 1964, earthquake is also indicated. The 3000-m bathymetric contour is from *Mammerickx and Smith* [1982]. Identified magnetic lineations are from *Drummond* [1981]. See Figure 6 for further explanation.

crust. The July 1, 1974, earthquake is consistent with this model; it clearly occurred in the crust (3 km centroid depth), and the thrust faulting mechanism has a *P* axis nearly perpendicular to the spreading direction. The September 11, 1975, thrust event is also shallow (5 km centroid depth). The other examples of thrust faulting for which we have accurate depths are at or below the Moho, although none is more than 10 km below the seafloor (Figure 4).

Thermoelastic stresses related to cooling of the lithosphere are thus consistent with the depth and age extent of near-ridge earthquakes and can account for the observation of deep normal faulting and at least some shallow thrust faulting. The higher level of near-ridge seismicity in general and of deep normal faulting in particular in certain portions of the central Indian Ocean, however, still requires that additional local processes act to accentuate the typical rate of stress release.

#### SECONDARY CONVECTION BENEATH YOUNG OCEANIC LITHOSPHERE?

One process which could play an important role in modifying the near-ridge stress regime in some areas is secondary convection immediately below the lithosphere [*Richter*, 1973; *Richter and Parsons*, 1975; *Buck*, 1984]. Secondary convection will obviously perturb the geotherm relative to simple plate cooling, thus inducing thermoelastic stresses. In addition, the state of stress may be affected directly through tractions applied to the base of the lithosphere.

Geoid height data derived from Seasat altimetry have recently been interpreted to support the existence of small-scale convection beneath young lithosphere of the Pacific plate [*Haxby and Weissel*, 1983]. Similar features may be present in regions of young lithosphere on the Indian plate (J. K. Weissel, personal communication, 1983); in particular, linear geoid anomalies interpreted as signatures of convective rolls oriented parallel to the direction of spreading are apparently observed in approximately the same area as the near-ridge earth-

quakes on the Indian plate side of the SEIR (Figure 5). Similar geoid patterns are not observed on the Antarctic side. Further, numerical models of convection in a variable-viscosity asthenosphere [*Buck*, 1984] demonstrate the possibility that small-scale convection may initiate by boundary layer instability beneath lithosphere similar in age to that of the near-ridge earthquakes in the Pacific and Indian plates. These findings suggest that the role of small-scale convection in modifying the state of stress in young oceanic lithosphere is a topic deserving of further attention.

#### TECTONIC EVOLUTION OF YOUNG OCEANIC LITHOSPHERE

In this section we draw together a number of observations concerning near-ridge earthquakes and consider some of the broader tectonic implications for the evolution of young oceanic lithosphere.

##### *Influence of Other Plate Boundaries*

We have assumed that near-ridge earthquakes are generally related to tectonic processes associated with the early evolution of the oceanic lithosphere created at the nearby spreading center, but in some cases the stresses arising from processes at other plate boundaries may also be significant. The most likely such case in our set of earthquakes occurs in the eastern Pacific, in the vicinity of the Panama Fracture Zone (Figure 10). All four events in this area with known mechanisms are characterized by right-lateral strike-slip motion on planes striking roughly north-south. The relatively frequent occurrence of near-ridge earthquakes in this region and the uniformity of the focal mechanisms may reflect the significance of stresses related to the nearby Central and South American convergence zones [*Pennington*, 1981]. Another region of concentrated near-ridge seismicity is near the intersection of the East Pacific Rise and the Cocos-Nazca spreading boundary (Figure 11); the seismicity in this area, however, appears to be associated only with one arm of the triple junction. Also, as

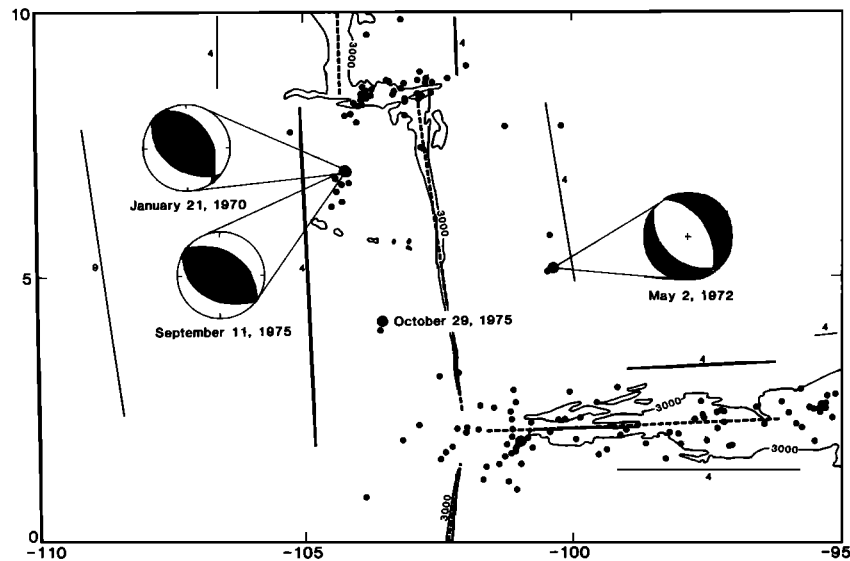


Fig. 11. Bathymetry, seismicity, and isochrons in the epicentral region of the January 21, 1970; May 2, 1972; and September 11, 1975, earthquakes, near the East Pacific Rise. The 3000-m bathymetric contour is from *Mammerickx and Smith* [1982]. See Figure 6 for further explanation.

noted above, the marked concentration of near-ridge seismicity at several sites in the central Indian Ocean may reflect the influence of stresses related to the continental convergence between India and Asia [Bergman et al., 1984], but the distance involved is quite large and the relationship must be considered speculative.

#### *Aseismicity of the Oceanic Crust*

One of the more striking features of the earthquakes for which we have reliable depths is the low level of seismicity in the oceanic crust. The only event which is clearly located in the crust (July 1, 1974, at a depth of 3 km) is also one of the smallest. Some of the larger events at greater depth may have ruptured into the crust, but it is difficult to avoid the conclusion that either the source of the seismogenic stress lies within the upper mantle or the crust is much weaker than the uppermost mantle (or both).

Studies of continental seismicity have indicated a tendency for hypocenters to cluster at two depths, in the upper crust and just below the Moho [Meissner and Strehlau, 1982; Chen and Molnar, 1983]. This observation has been interpreted in terms of very different ductile flow laws for crustal and mantle materials. With reasonable assumptions as to the thermal structure and strain rate, the relative strength of the lower continental crust may be substantially reduced by ductile flow, producing a strength envelope with two peaks, one in the upper crust and another just below the Moho. Diabase is often chosen as an analog for the oceanic crust, but diabase remains entirely in the brittle field under the pressure and temperature conditions in the near-ridge oceanic crust [Caristan, 1982]. A single-peaked strength envelope (such as in Figure 7) is thus predicted, and it is difficult to explain the concentration of near-ridge seismicity just below the Moho. One possibility is that a material considerably weaker than diabase, perhaps because of hydrothermal alteration, is a more appropriate choice to represent the strength of the oceanic crust in near-ridge environments [e.g., Epp and Suyenaga, 1978].

The thermoelastic stress hypothesis provides an alternative explanation for the relative aseismicity of oceanic crust. The bimetallic strip analog for the oceanic lithosphere [Turcotte, 1974], as discussed above, predicts a concentration of thermoelastic stress in the upper mantle, just below the Moho. Furthermore, if thermoelastic stresses resulting from plate cooling are considered as a significant source of stress in young oceanic lithosphere, the aseismicity of the oceanic crust may be attributed to the prior relief of those stresses near the ridge axis by cooling and cracking associated with hydrothermal circulation [Lister, 1977], provided that this circulation extended at least to the base of the crust.

#### *Transition From Ridge Axis to Intraplate Stress Regime*

There is no evidence in the data assembled here for the proposed transition from horizontal extension to compression at an age of about 20 m.y. [Sykes and Sbar, 1974]. Large thrust-faulting events are observed in lithosphere as young as 3 m.y., while normal faulting is observed at ages up to 35 m.y. (Figure 4). While normal faulting is not observed in oceanic lithosphere older than 35 m.y., except in the presence of large bending stresses seaward of subduction zones [e.g., Chapple and Forsyth, 1979], none of the near-ridge normal-faulting events resembles a ridge axis earthquake in terms of focal depth or (with one exception) *T* axis orientation. The transition from teleseismically identifiable extensional faulting in the direction of plate motion apparently occurs very soon after plate creation. The use of a general transition in the stress field at 20 m.y. age, from extension parallel to the spreading direction to compression in the same direction [Fleitout and Froidevaux, 1983], is not justified by the source mechanism data of this study.

#### *Near-Ridge Earthquakes and "Ridge Push"*

We see little evidence to suggest that a "ridge push" compressive stress associated with subsidence of the cooling lithosphere [Lister, 1975; Dahlen, 1981] is a dominant component of the deviatoric stress released by near-ridge earthquakes.

The only support for this hypothesis comes from two earthquakes (November 25, 1965, and May 9, 1971) which are characterized by thrust faulting with the  $P$  axis oriented nearly perpendicular to the nearby ridge axis.

A  $P$  axis oriented along the spreading direction is not, however, a general feature of near-ridge thrust events. Figure 11 shows a short length of the East Pacific Rise near which several earthquakes have occurred. On the Pacific plate side, two large thrust events occurred about 5 years apart in the same location. The focal mechanisms of these events are very well constrained by the body wave inversion and are essentially identical. The  $P$  axes for these events make an angle of approximately  $30^\circ$  with the spreading direction. On the Cocos plate side of the ridge occurred a normal-faulting earthquake with a  $T$  axis parallel to the  $P$  axes of the two thrust events. Another event on the Pacific plate side, which we were unable to study because of contamination of the body waves by an earlier event, is also characterized by normal faulting (D. A. Wiens, personal communication, 1983). We see no possibility of accounting for these events with either horizontal principal stress oriented perpendicular to the ridge.

The only other thrust-faulting earthquake for which we obtained a focal mechanism by body wave inversion (July 1, 1974) has a  $P$  axis nearly perpendicular to the spreading direction. Further, none of the remaining events in Table 1 with proposed thrust-faulting mechanisms provides convincing evidence of the importance of ridge-perpendicular compressive stress. All the strike-slip events have one nodal plane parallel to the local trend of fracture zones; thus their inferred  $P$  axes are also oblique to the spreading direction.

The lack of a clear influence of "ridge push" on the state of stress near mid-ocean ridge systems permits a lower bound to be placed on the typical level of stress differences in young oceanic lithosphere if the assumption is made that the stress difference is nearly zero at the ridge axis [e.g., *Artyushkov*, 1973; *Dahlen*, 1981]. Under this assumption, the stress difference in the upper 20 km increases approximately as the square root of age to 200–400 bars at 30 m.y. age [*Dahlen*, 1981]. The typical stress differences in young oceanic lithosphere must significantly exceed this value; i.e., stress differences of a few hundred bars or greater must be present in the regions of near-ridge earthquake hypocenters.

#### CONCLUSIONS

We present in this paper a synthesis of the locations and styles of faulting of earthquakes occurring in young oceanic lithosphere (2.5–35 m.y. old) near oceanic spreading center systems. For 32 such earthquakes we determined the parameters of the best fitting point-source double-couple mechanisms, using a formal inversion technique based on matching synthetic and observed  $P$  and  $SH$  waveforms [*Nabelek*, 1984].

Near-ridge earthquakes occur along all major mid-ocean ridge systems, but the central Indian Ocean is unusually active. There is no correlation between the levels of ridge axis and near-ridge seismicity. Most of the moment release occurs in lithosphere less than 15 m.y. old.

All faulting types are observed for near-ridge earthquakes. Thrust faulting is observed in lithosphere as young as 3 m.y., and normal faulting is observed in lithosphere as old as 35 m.y. Near-ridge normal-faulting is characterized by a  $T$  axis that is oblique or perpendicular to the local spreading direction. Strike-slip faulting in young oceanic lithosphere frequently occurs on or near fracture zones, but the sense of slip is in the same sense as the offset of the ridge segments, op-

posite to that expected for a transform fault. The  $P$  axes of strike-slip and thrust-faulting events are, in general, not perpendicular to the strike of the ridge, as would be expected if "ridge push" were an important source of the stress released in the earthquakes. This observation allows a lower bound of several hundred bars to be placed on the typical level of differential stress in young oceanic lithosphere.

Most near-ridge seismicity occurs at depths of 5 km or more below the seafloor, in the uppermost mantle. No thrust-faulting events are observed at depths greater than 10 km, however. The deepest events in young oceanic lithosphere, up to 20 km below the seafloor, are generally characterized by normal faulting. They occur at depths at which standard thermal models predict temperatures up to  $800^\circ\text{C}$ . The tectonic strain rate associated with the deepest normal faulting is locally at least  $10^{-15} \text{ s}^{-1}$ . Several features of the distribution of hypocenters and focal mechanisms of the near-ridge earthquakes may be most easily explained if thermoelastic stress related to plate cooling is an important source of stress in the near-ridge environment.

The relative abundance and consistent strike-slip focal mechanisms of near-ridge earthquakes in a small region of the eastern Pacific, near the Cocos-Nazca plate boundary, may reflect the presence of significant stresses associated with the nearby Central and South American convergent boundaries. The higher level of near-ridge normal-faulting seismicity in portions of the Indian Ocean may be speculatively attributed to the enhancement or modification of thermoelastic stresses by processes associated with the continental collision between India and Asia or by the presence of active small-scale convection beneath young lithosphere of the Indian plate.

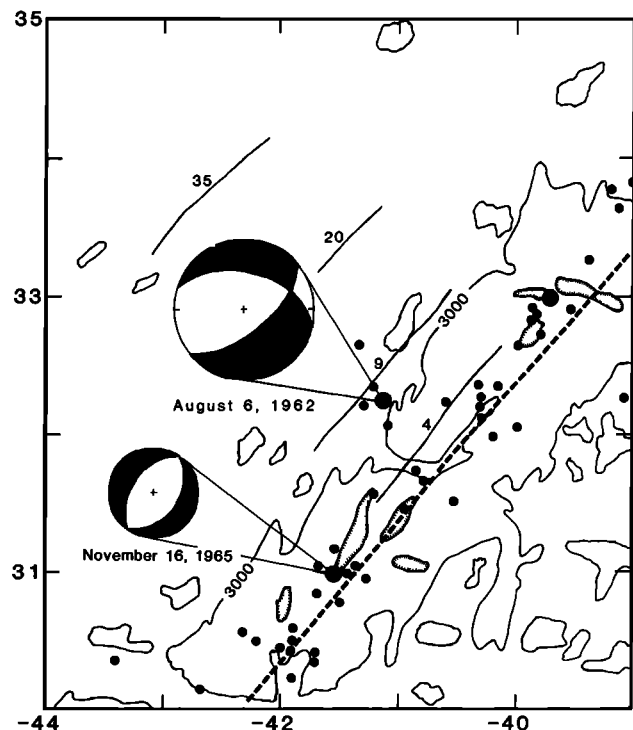


Fig. A1. Bathymetry, seismicity, and isochrons in the epicentral region of the August 6, 1962, earthquake, near the Mid-Atlantic Ridge. The 3000-m bathymetric contour is from *Searle et al.* [1982]. Also shown is the focal mechanism of a ridge-axis earthquake (November 16, 1965) determined with the body waveform inversion technique used in this paper [*Huang et al.*, 1984]. See Figure 6 for further explanation.

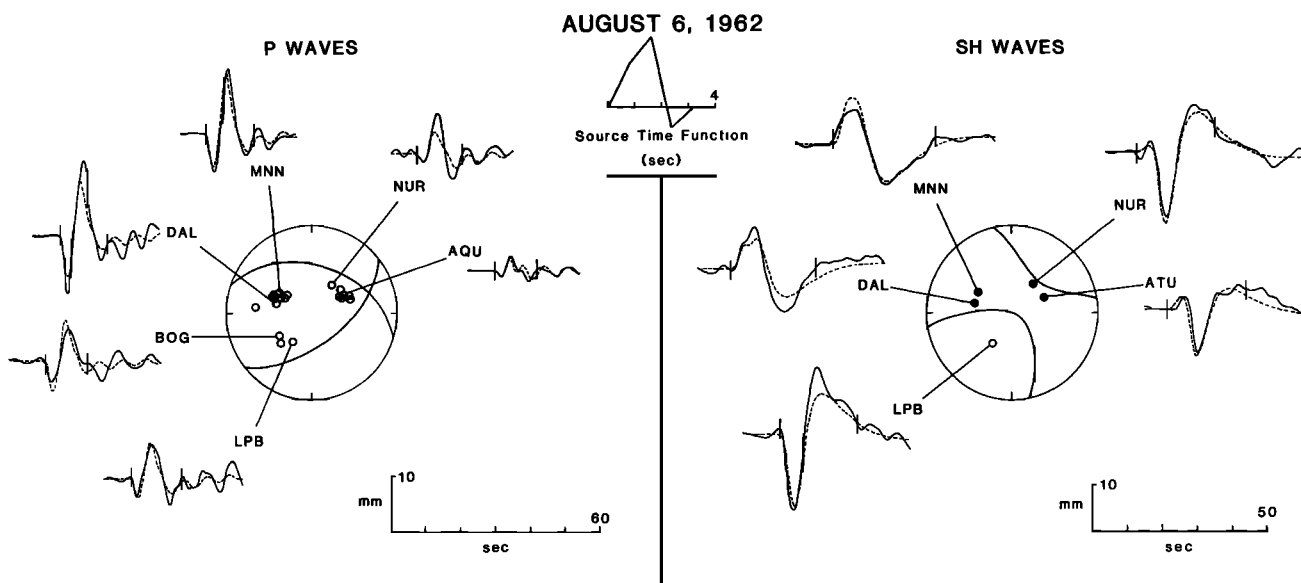


Fig. A2. Comparison of observed (solid line) and synthetic (dashed line) long-period *P* and *SH* waves for the August 6, 1962, earthquake, with the focal mechanism solution obtained from the inversion plotted on the lower focal hemisphere (equal-area projection). All amplitudes are normalized to an instrument magnification of 3000; the amplitude scales correspond to the waveforms that would be observed on an original seismogram from such an instrument. The two vertical lines delimit the portion of each time series, digitized at 0.5-s intervals, used in the inversion. Symbols for both types of waves are open circle, dilatation; solid circle, compression; cross, emergent arrival. For *SH* waves, compression corresponds to positive motion as defined by *Aki and Richards* [1980]. Some first motions are shown for stations not used in the waveform inversion. The source time function obtained from the inversion is also shown.

APPENDIX: SOURCE MECHANISMS FROM LONG-PERIOD BODY WAVEFORM INVERSION

We present here the details of the source mechanisms determined from the inversion of *P* and *SH* waveforms. The inversion procedure follows the method of *Nabelek* [1984]. The source time function determined in the inversion is composed of a series of overlapping triangular elements. The convention for describing a double-couple source mechanism is that of *Aki and Richards* [1980]: we specify the strike and dip of one nodal plane and the slip angle, which defines the motion of the

hanging wall relative to the footwall, measured counterclockwise from strike on the foot wall. The three angles are given in the order: strike/dip/slip. Focal depths are relative to the sea-floor.

Nine of the earthquake mechanisms have been described by *Bergman et al.* [1984] and are not discussed further. Mechanisms for the remaining 23 events are presented below in chronological order. Following the date of each earthquake, the figure numbers for the map of the epicentral region and for the comparison of synthetic and observed seismograms are

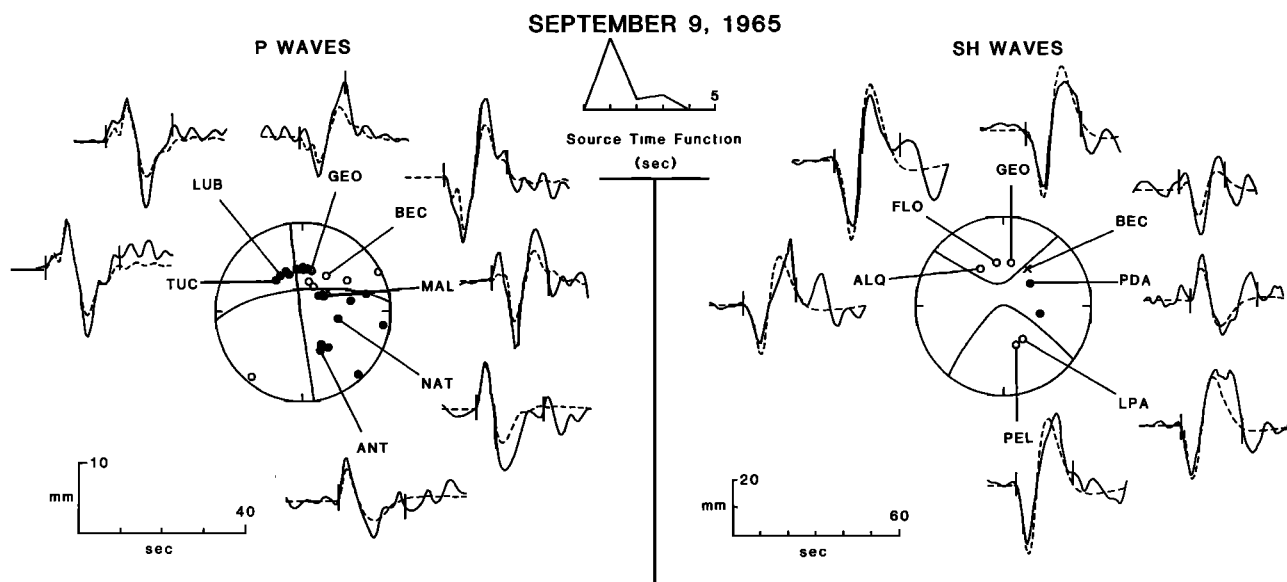


Fig. A3. Comparison of the observed and synthetic *P* and *SH* waves for the September 9, 1965, event. See Figure A2 for further explanation.

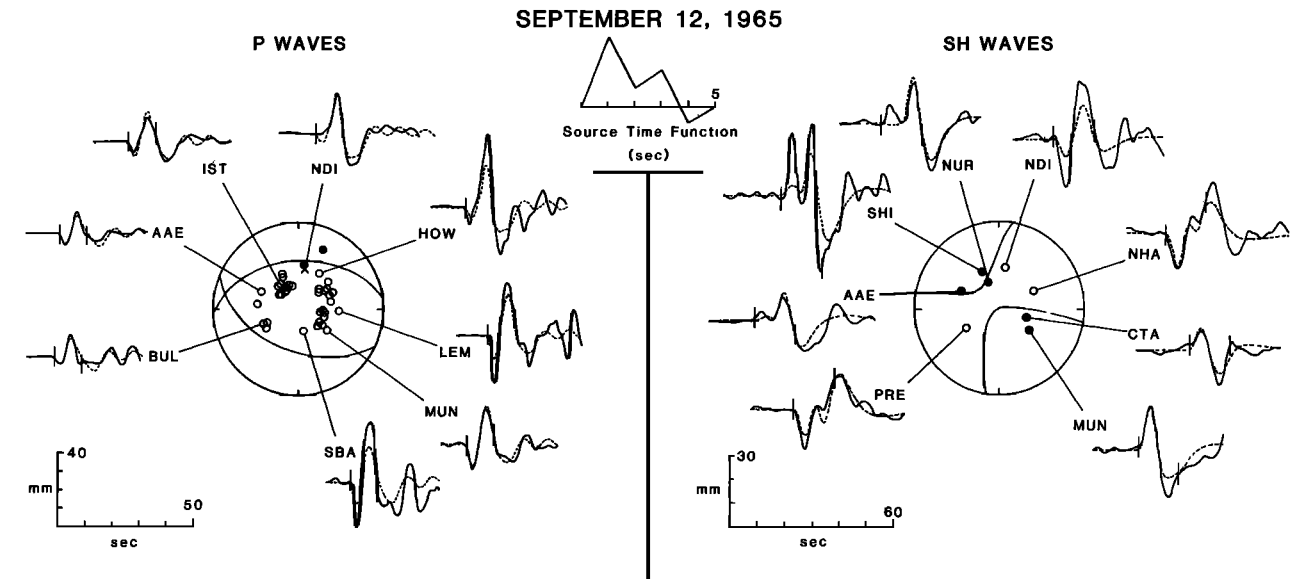


Fig. A4. Comparison of the observed and synthetic  $P$  and  $SH$  waves for the September 12, 1965, event. See Figure A2 for further explanation.

given in parentheses. The station codes and locations of seismograph stations used for the body waveform inversions are given by *Poppe et al.* [1978].

#### August 6, 1962 (Figures A1 and A2)

*Sykes* [1967] reported a poorly constrained normal-faulting mechanism for this earthquake and treated it as a ridge axis event, although he later noted that the epicenter lies outside the rift valley, along a section of the Mid-Atlantic Ridge with no significant offsets [*Sykes*, 1970a]. The inversion solution (288/43/315) is essentially identical with *Sykes's* mechanism; it has a significant component of strike-slip motion and a  $T$  axis striking at an angle of  $63^\circ$  from the direction of spreading. The observed  $P$  and  $SH$  waves are well fit by this mechanism with a centroid depth of 10 km and a seismic moment of  $1.3 \times 10^{25}$  dyn cm. The emergent character of the  $SH$  wave at NUR is

clearly revealed in the unrotated horizontal component records.

#### September 9, 1965 (Figures 10 and A3)

*Molnar and Sykes* [1969] found a strike-slip focal mechanism with a significant component of thrust faulting (173/84/150) for this event on the flank of the Cocos Ridge. The inversion solution is similar but closer to pure strike slip (173/88/160) at a depth of 8 km and with a seismic moment of  $2.4 \times 10^{25}$  dyn cm. *Wiens and Stein* [1983a] estimated a depth of 7 km for this event, using *Molnar and Sykes's* mechanism. The nodal plane striking at  $173^\circ$ , subparallel to the trend of a fracture zone which intersects the ridge near the epicenter, is probably the fault plane.

#### September 12, 1965 (Figures 6 and A4)

*Banghar and Sykes* [1969] proposed a normal-faulting mechanism with a large component of strike-slip motion for this event (270/54/230). *Stein* [1978] found that the surface wave radiation patterns are better fit by a nearly pure normal-faulting mechanism (270/60/260), and he matched synthetic waveforms to the  $P$  waves to constrain the depth to about 15 km below the seafloor. *Stein* noted a significant discrepancy between the seismic moments inferred from the  $P$  waves ( $3.5 \times 10^{25}$  dyn cm) and the surface waves ( $6.8 \times 10^{25}$  dyn cm).

The body wave inversion solution is somewhat deeper (18 km) than that of *Stein* [1978], but the seismic moment ( $3.3 \times 10^{25}$  dyn cm) is close to the value *Stein* found from matching  $P$  waveforms. The best fitting double-couple mechanism (263/44/246) is intermediate between previously proposed mechanisms. In order to model the low amplitudes of the  $P$  waves in Africa (BUL and AAE) relative to stations such as SBA and MUN, the mechanism must have a larger component of strike-slip motion (slip angle of approximately  $240^\circ$ ) than the focal mechanism suggested by *Stein* [1978], but the mechanism of *Banghar and Sykes* [1969] results in significant misfit to the observed  $SH$  waves at three stations to the northwest (AAE, SHI, and NUR). The prominent positive motion of the direct  $S$  wave at these stations requires a slip angle of

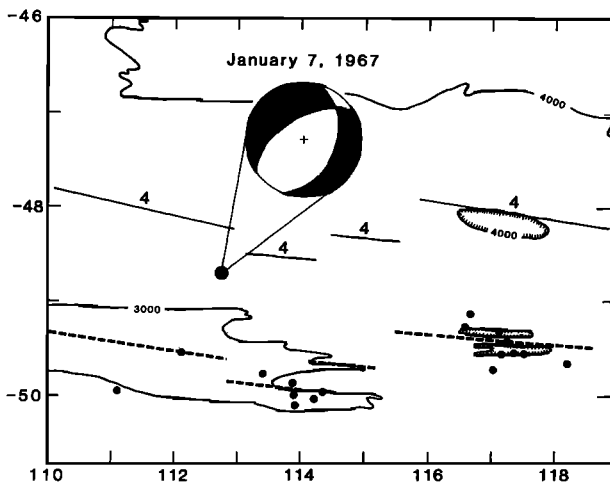


Fig. A5. Bathymetry, seismicity, and isochrons in the epicentral region of the January 7, 1967, earthquake, south of Australia. Bathymetric contours (3000 and 4000 m) are from *Hayes and Vogel* [1981], *Falconer and Tharp* [1981], and *Fisher et al.*, [1982]. See Figure 6 for further explanation.

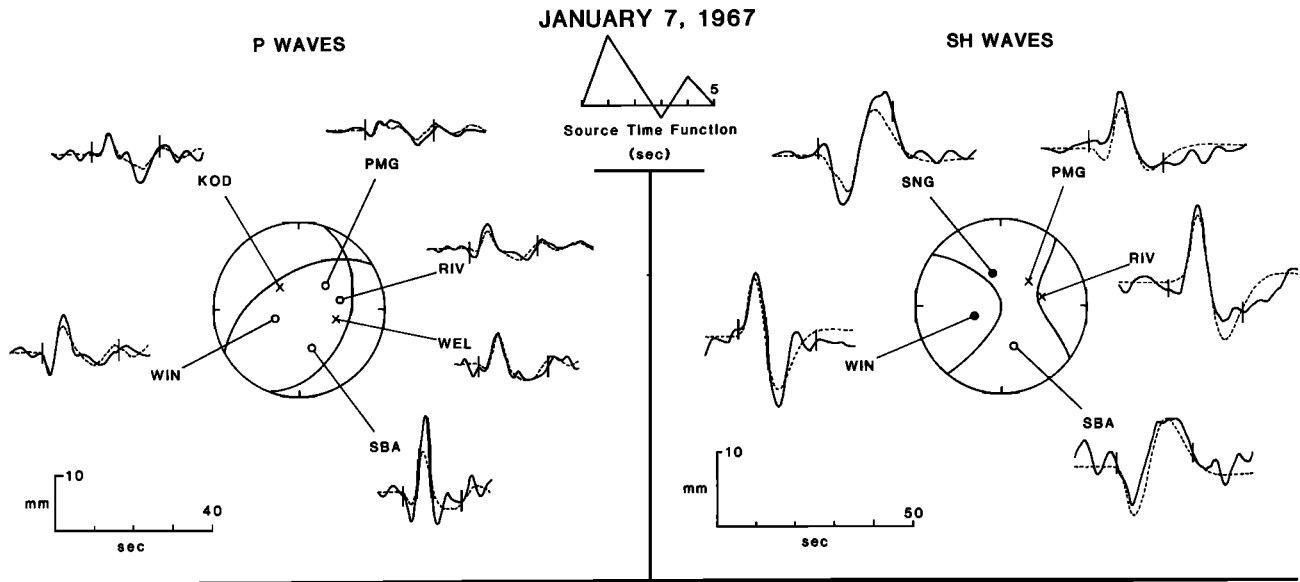


Fig. A6. Comparison of the observed and synthetic *P* and *SH* waves for the January 7, 1967, event. See Figure A2 for further explanation.

approximately  $260^\circ$ , as do the surface waves. The horizontal component seismograms at PRE were found to have reversed polarity; the *SH* waveform was corrected prior to the inversion.

January 7, 1967 (Figures A5 and A6)

One nodal plane of the focal mechanism (16/41/236) for this earthquake, near a small-offset fracture zone of the SEIR, is subparallel to the fracture zone trend of  $N15^\circ E$ . The mechanism has a significant component of strike-slip motion in the same sense as the ridge offset. A pure normal-faulting mechanism would not account for the differences between the *P* waves at WIN and PMG. The emergent nature of the *SH* wave at PMG is well determined: both observed horizontal components break clearly, but when they are rotated to the transverse component, the direct *S* wave is cancelled. The emergent *SH* wave at RIV is a similar case. At SNG, both

observed components break clearly upward, as the *SH* wave does, but the inversion solution shows a small dilatation for the direct phase. The correct starting point for the *SH* wave at WIN is not clear on the observed records; the small positive motion prior to the main pulse may simply be noise. Using an earlier starting point for WIN (i.e., assuming the direct phase is nodal) results in a poor fit at all stations. The seismic moment of this earthquake is  $1.2 \times 10^{25}$  dyn cm, and the centroid depth is 9 km.

November 10, 1967 (Figures 6 and A7)

This earthquake occurred on the west flank of the Chagos Bank only one day before an unusual swarm of normal-faulting earthquakes [Stein, 1978]. The focal mechanism of this event, however, is characterized by nearly pure strike-slip faulting (234/76/191), in a right-lateral sense on the northeast striking nodal plane, parallel to the strike of local fracture

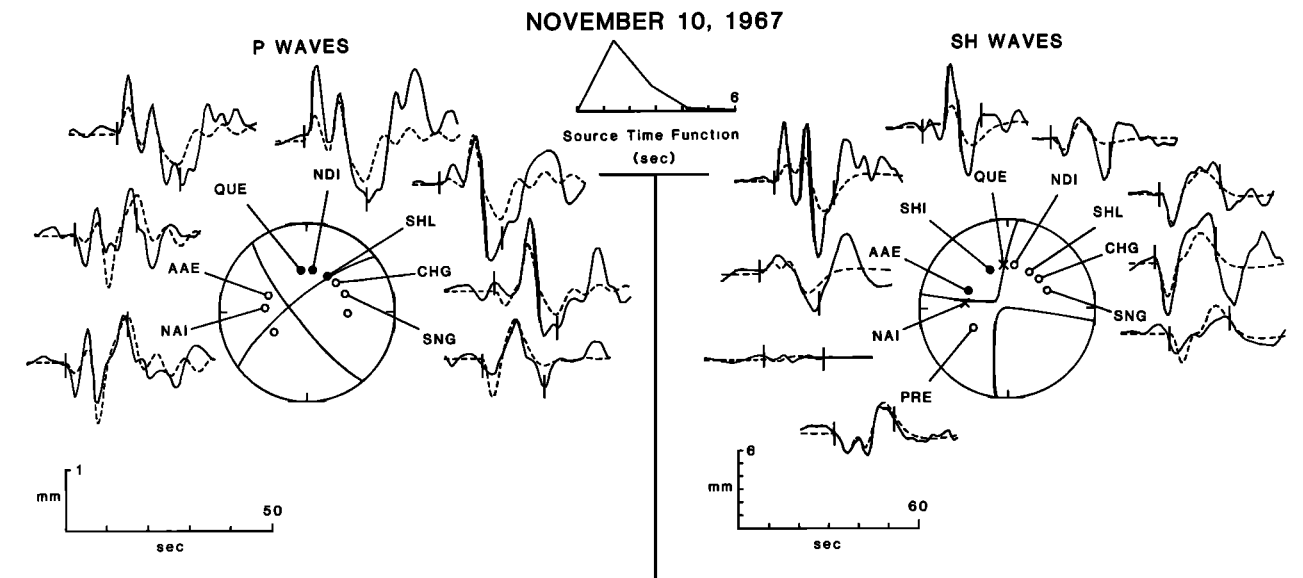


Fig. A7. Comparison of the observed and synthetic *P* and *SH* waves for the November 10, 1967, event. See Figure A2 for further explanation.

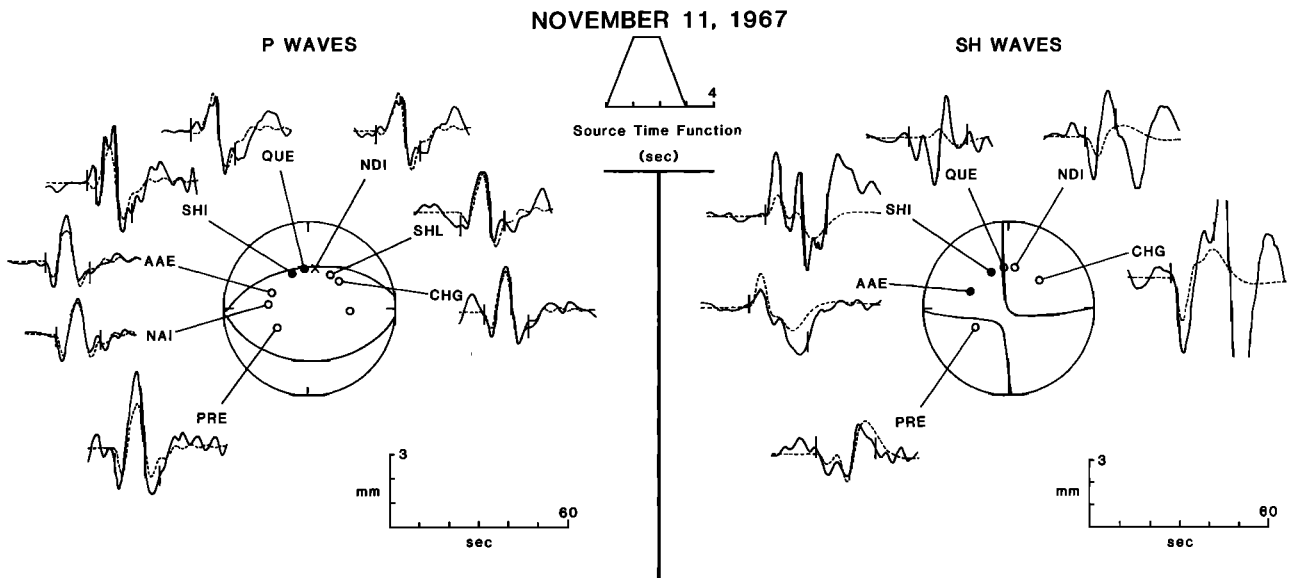


Fig. A8. Comparison of the observed and synthetic *P* and *SH* waves for the November 11, 1967, event. See Figure A2 for further explanation.

zones. The *P* wave polarities could be fit with a normal-faulting mechanism (e.g., 270/60/270), but the fit of the synthetics to the observed waveforms with such a mechanism is very poor. The basic shapes of both the *P* and *SH* waves are well fit with the strike-slip solution at a depth of 18 km and with a seismic moment of  $3.0 \times 10^{24}$  dyn cm. Many details of the waveforms are not reproducible, however. The horizontal component seismograms at PRE were found to have reversed polarity; the *SH* waveform was corrected prior to the inversion.

*November 11, 1967 (Figures 6 and A8)*

This earthquake is the first event in the swarm of normal-faulting earthquakes studied by Stein [1978]. By fixing one

nodal plane on the basis of *P* wave first motions and constraining the slip angle with surface waves, Stein obtained a pure normal-faulting mechanism (280/65/270) with a seismic moment of  $4.5 \times 10^{24}$  dyn cm. The inversion solution is also characterized by normal faulting but with a different strike (264/50/261). The strike is not very well constrained by the first motions of the emergent *P* waves to the north but is controlled mostly by the *SH* waves. A strike of  $280^\circ$  would produce a nodal arrival for the *SH* wave at NDI instead of the observed strong dilatation. The horizontal component seismograms at PRE were found to be reversed; the *SH* waveform was corrected prior to the inversion. The overall fit of the *SH* waves is mediocre at best. The inversion yields a depth of 17 km and a seismic moment of  $3.7 \times 10^{24}$  dyn cm.

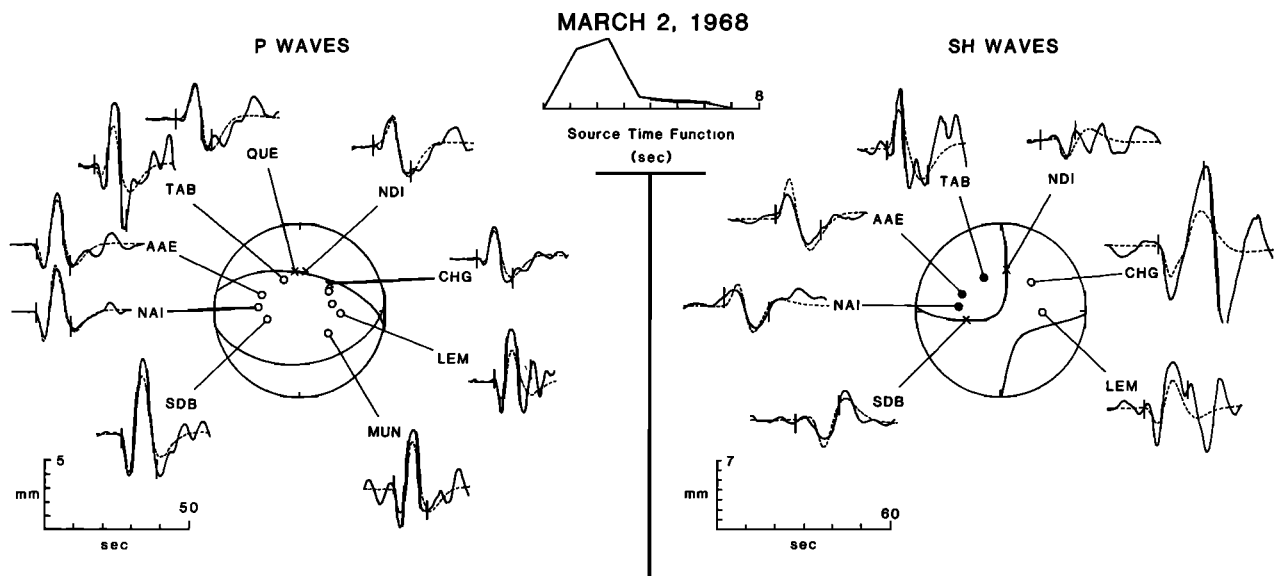


Fig. A9. Comparison of the observed and synthetic *P* and *SH* waves for the March 2, 1968, event. See Figure A2 for further explanation.

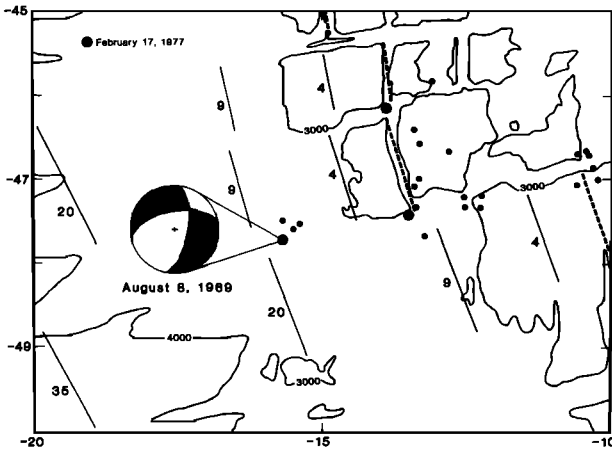


Fig. A10. Bathymetry, seismicity, and isochrons in the epicentral region of the August 8, 1969, earthquake, near the South Atlantic Ridge. Bathymetric contours (3000 and 4000 m) are from *LaBrecque and Rabinowitz* [1981]. The epicenter of another near-ridge event from Table 1 (February 17, 1977) is also shown. See Figure 6 for further explanation.

*March 2, 1968 (Figures 6 and A9)*

Using the same approach as for the November 11, 1967, event discussed above, *Stein* [1978] found a normal-faulting solution for this event (280/60/270) with a seismic moment of  $8.8 \times 10^{24}$  dyn cm. The inversion solution (284/52/280,  $M_0 = 7.7 \times 10^{24}$  dyn cm) is in very close agreement with Stein's results. The later portions of several of the *SH* waves (e.g., NDI, CHG, LEM) are disturbed, possibly by contamination from the large *SV* waves generated by a dip-slip event, but the early portions of the waveforms are fit reasonably well. The emergent nature of the *SH* wave at SDB (which is naturally rotated onto the N-S component) is confirmed by the clear arrival of *SV* energy at that time on the E-W component. The centroid depth is 13 km.

*August 8, 1969 (Figures A10 and A11)*

This earthquake is on a fracture zone west of a major offset of the Mid-Atlantic Ridge. *Forsyth* [1975] found a strike-slip mechanism (8/74/200) from *P* wave first motions. The inversion solution (8/67/215) is similar, except that it has a larger component of normal faulting. The sense of slip on the nodal plane parallel to the fracture zone is the same as the offset of the ridge. The horizontal component seismograms at TRN were found to be reversed; the *SH* waveform was corrected prior to the inversion. The centroid depth is 7 km, and the seismic moment is  $1.5 \times 10^{25}$  dyn cm.

*January 21, 1970 (Figures 11 and A12)*

*Anderson et al.* [1974] reported a normal-faulting mechanism for this event. *Bergman and Solomon* [1980] found that a thrust fault solution provides a good fit to the first motions, but the position of one of the nodal planes was unconstrained. The inversion solution is characterized by thrust faulting (332/41/106) with a centroid depth of 6 km and a seismic moment of  $1.4 \times 10^{26}$  dyn cm. We found only three usable *SH* waves for this event because the huge *SV* waves caused the horizontal components to be clipped at many stations. The later part of the *SH* wave at PEL is quite disturbed, but the inversion converges to the same solution even if this station is given no weight. The *P* waves are well fit by the point source synthetics, despite the size of this event.

*March 31, 1970 (Figures 6 and A13)*

*Sykes and Sbar* [1974] reported a large number of first motion polarities which apparently constrain the mechanism of this event to a combination of strike-slip and normal faulting (260/57/220), but this mechanism results in a poor fit to the observed *P* and *SH* waveforms. The horizontal component seismograms at PRE and NIL were found to have reversed polarity; the *SH* waveforms were corrected prior to the inversion. A good fit to the *SH* waves and most of the *P* waves is obtained in the inversion solution (43/83/187), which is characterized by right-lateral strike-slip motion on a northeast

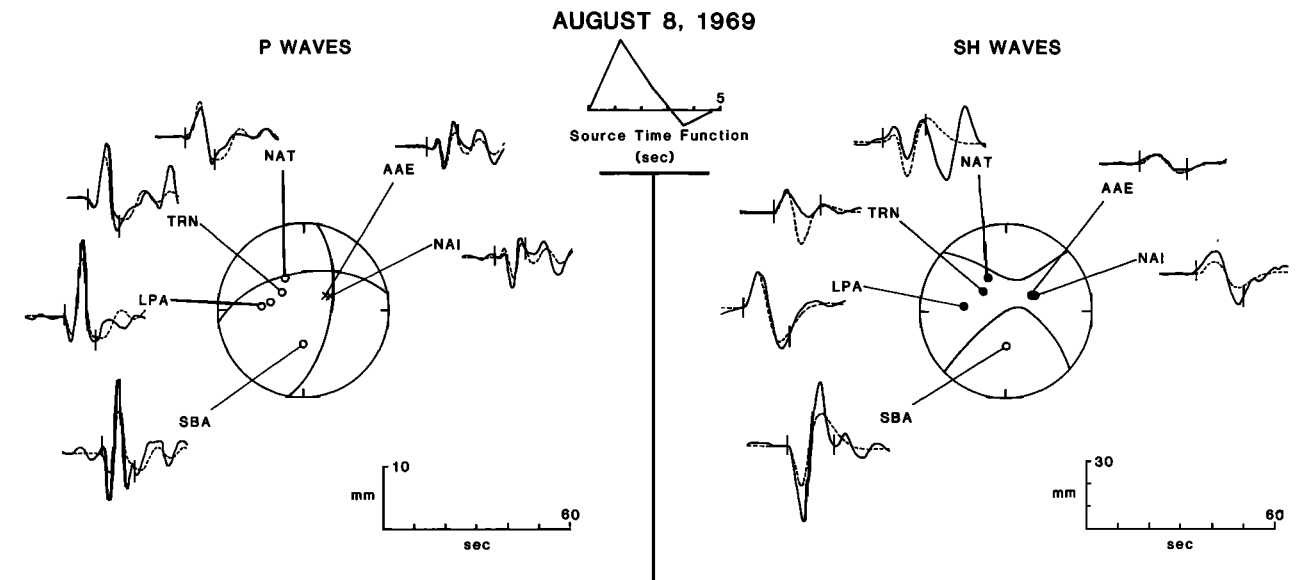


Fig. A11. Comparison of the observed and synthetic *P* and *SH* waves for the August 8, 1969, event. See Figure A2 for further explanation.

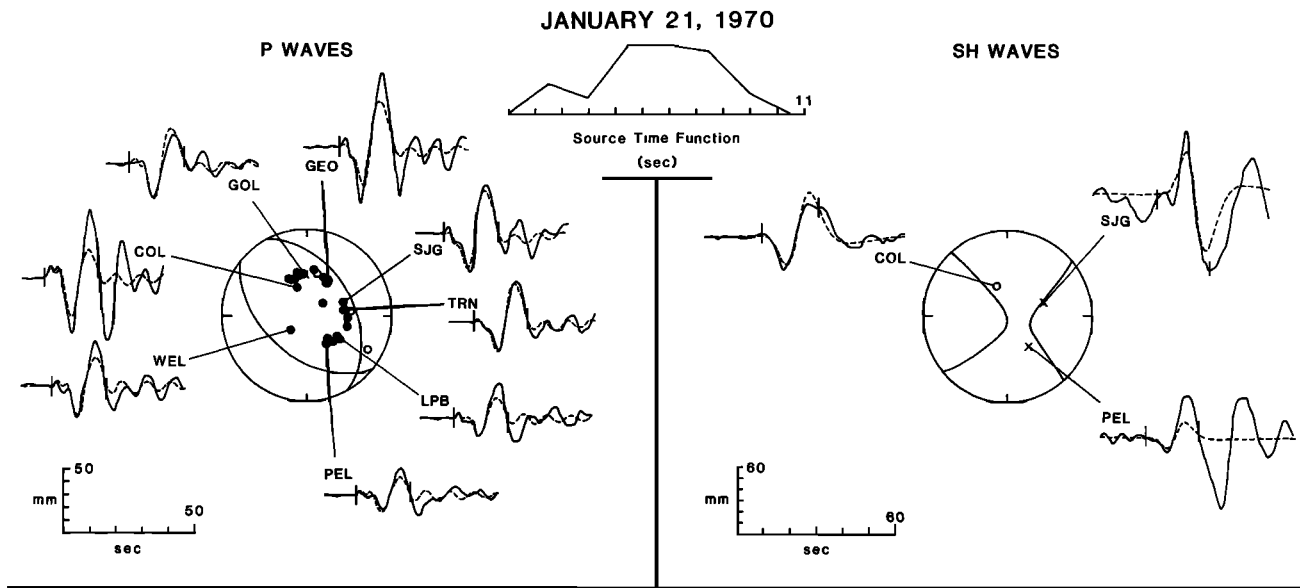


Fig. A12. Comparison of the observed and synthetic *P* and *SH* waves for the January 21, 1970, event. See Figure A2 for further explanation.

striking nodal plane that parallels the strike of local fracture zones. The observed distribution of first motion polarities is best fit by a mechanism of approximately 216/85/185, but such a mechanism provides a very poor fit to the *SH* waveforms at NIL and MSH. The *P* waveform at SNG (and several other stations to the east) is incompatible with the point source solution that best fits the remaining *P* waves and *SH* waves. The source of the discrepancy is not readily apparent, but complexities in the rupture process presumably contribute. The depth is 13 km, and the seismic moment is  $8.0 \times 10^{24}$  dyn cm.

April 25, 1970 (Figures 6 and A14)

An exceptionally good fit to both *P* and *SH* waves for this earthquake was obtained with a strike-slip focal mechanism

(248/85/192) which is similar to that of the March 31, 1970, event. The horizontal component seismograms at PRE were found to have reversed polarity; the *SH* waveforms were corrected prior to the inversion. The seismic moment is  $1.6 \times 10^{24}$  dyn cm, and the centroid depth is 11 km.

May 9, 1971 (Figures A15 and A16)

This event was first studied by Forsyth [1973], who used *P* wave first motion polarities and the radiation pattern of Rayleigh waves to infer a thrust-faulting mechanism (196/60/90) with the *P* axis roughly perpendicular to the ridge axis. Forsyth proposed a shallow depth (<10 km). Wiens and Stein [1983a] obtained a depth of 8 km by matching synthetics to

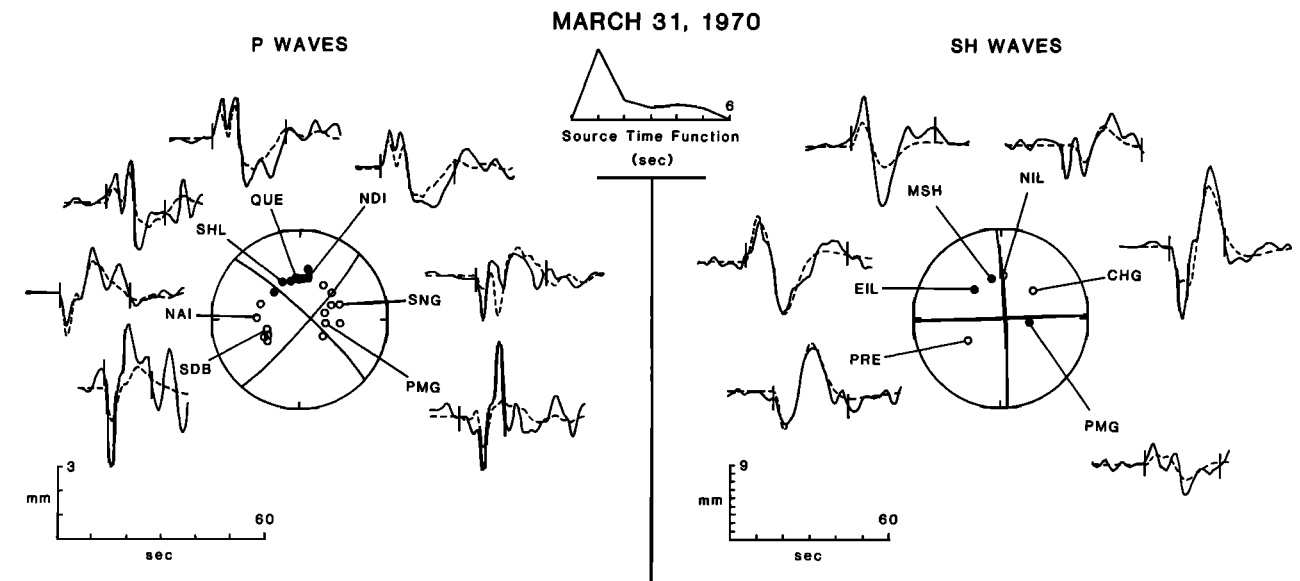


Fig. A13. Comparison of the observed and synthetic *P* and *SH* waves for the March 31, 1970, event. See Figure A2 for further explanation.

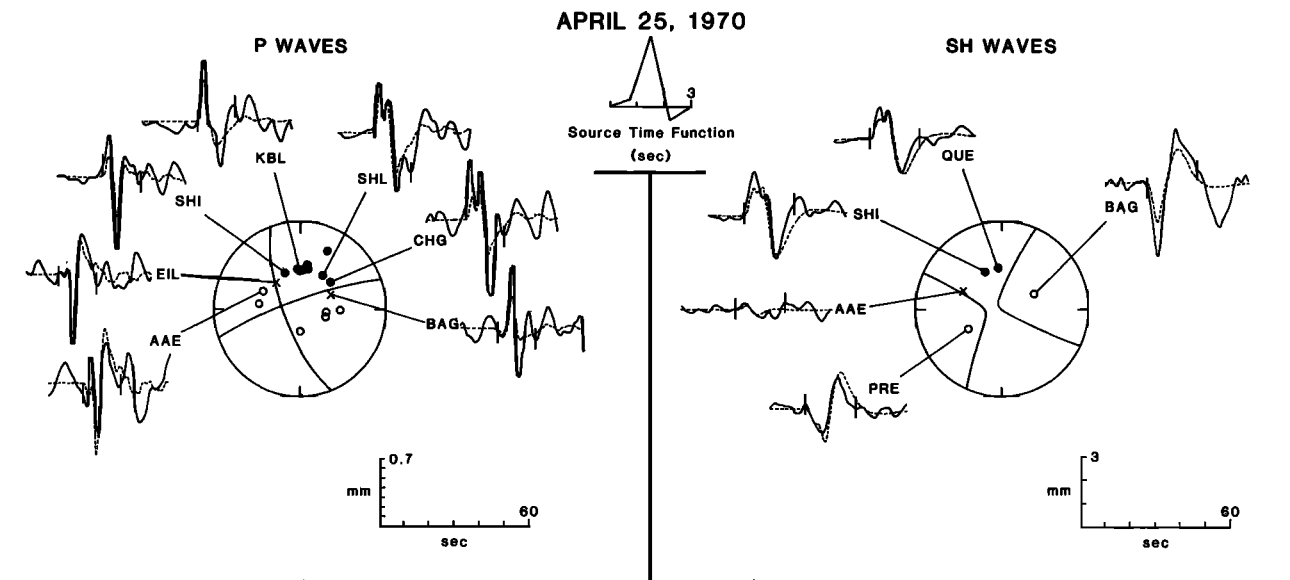


Fig. A14. Comparison of the observed and synthetic *P* and *SH* waves for the April 25, 1970, event. See Figure A2 for further explanation.

the observed *P* waves, using Forsyth's mechanism. The inversion solution is consistent with the multiple source model used by Wiens and Stein [1983a] to match the observed *P* waves. We performed the inversion twice, once with three separate point sources (also inverting for the relative timing of the subevents) and once with a single source but with a time function long enough to include all the subevents. The multiple source model offers no improvement over the single source model. The source process of this earthquake is well described by a single rupture geometry with three distinct episodes of faulting (25/46/104). The mechanism is similar to Forsyth's, at a depth of 9 km and with a total moment of  $5.3 \times 10^{25}$  dyn cm. Earthquakes characterized by multiple ruptures are generally very difficult to model, but the synthetic seismograms for this event provide an exceptionally good fit to the observed body waves.

#### May 2, 1972 (Figures 11 and A17)

For this earthquake, Anderson *et al.* [1974] reported a normal-faulting mechanism very similar to the inversion solution (332/49/280). The *SH* waves are not very well recorded, but the synthetic waveforms match the overall character of the observed records at most stations. The depth is 11 km, and the seismic moment is  $1.8 \times 10^{25}$  dyn cm.

#### June 29, 1973 (Figures 10 and A18)

Station coverage for this small event is poor, but the observed waveforms are very well fit by a combination thrust/strike-slip mechanism (353/61/169) at a depth of 6 km, near the base of the oceanic crust. The seismic moment is  $2.6 \times 10^{24}$  dyn cm. The nodal plane striking at  $N7^\circ W$  is sub-parallel to the fracture zone in the epicentral region. The much larger nearby earthquake of March 29, 1976, has only a vaguely similar mechanism.

#### November 17, 1973 (Figures 6 and A19)

A very good fit to observed *P* and *SH* waveforms from this earthquake is obtained with a mechanism characterized by a combination of normal and strike-slip faulting (46/51/226). At a depth of 20 km, this is the deepest event in this study. The seismic moment is  $4.8 \times 10^{24}$  dyn cm.

#### July 1, 1974 (Figures A20 and A21)

This event is the largest of a cluster of earthquakes which have occurred within a small region of the African plate in the South Atlantic. The epicenter is apparently on a zero-offset fracture zone [Schouten and White, 1980]. The small size and remoteness of this event make it difficult to obtain good station coverage for the inversion, but the available records are of high quality. The inversion solution is characterized by nearly pure thrust faulting (68/29/92) at a very shallow depth (3 km). The *P* axis of this event is nearly perpendicular to the direction of spreading. The seismic moment is  $3.3 \times 10^{24}$  dyn cm.

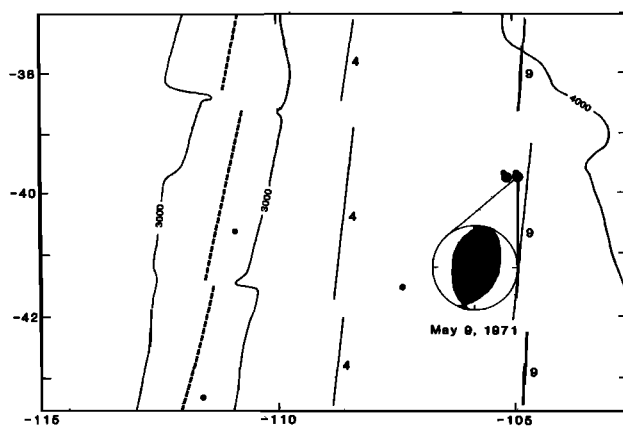


Fig. A15. Bathymetry, seismicity, and isochrons in the epicentral region of the May 9, 1971, earthquake, near the Pacific-Antarctic Ridge. Bathymetric contours (3000 and 4000 m) are from Mammerickx and Smith [1980]. See Figure 6 for further explanation.

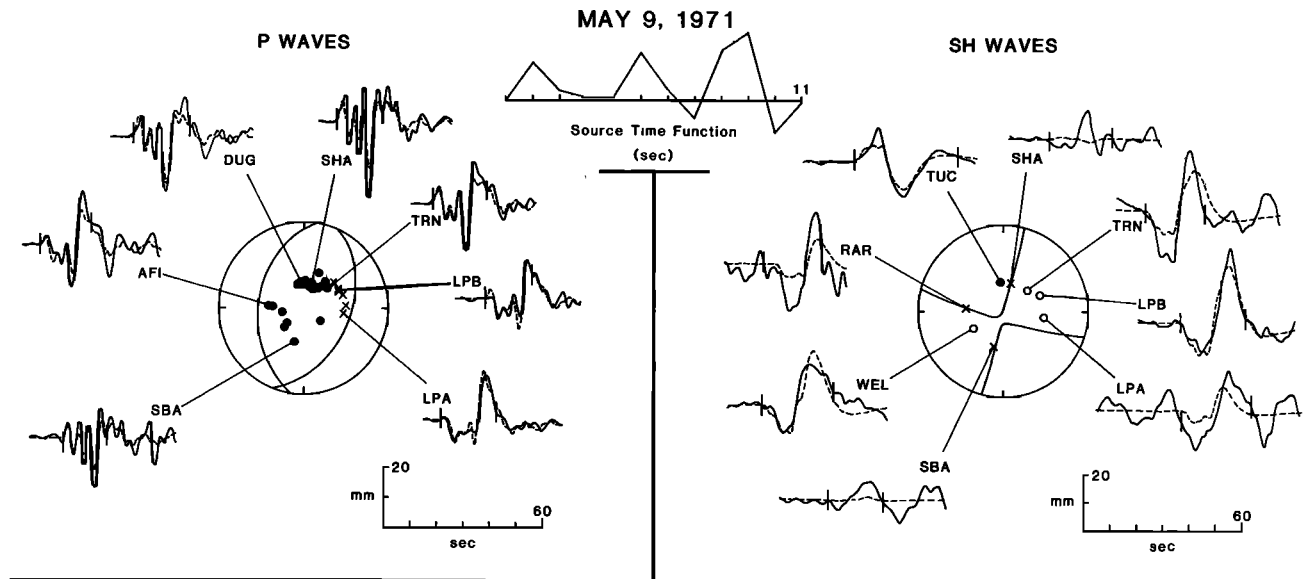


Fig. A16. Comparison of the observed and synthetic *P* and *SH* waves for the May 9, 1971, event. See Figure A2 for further explanation.

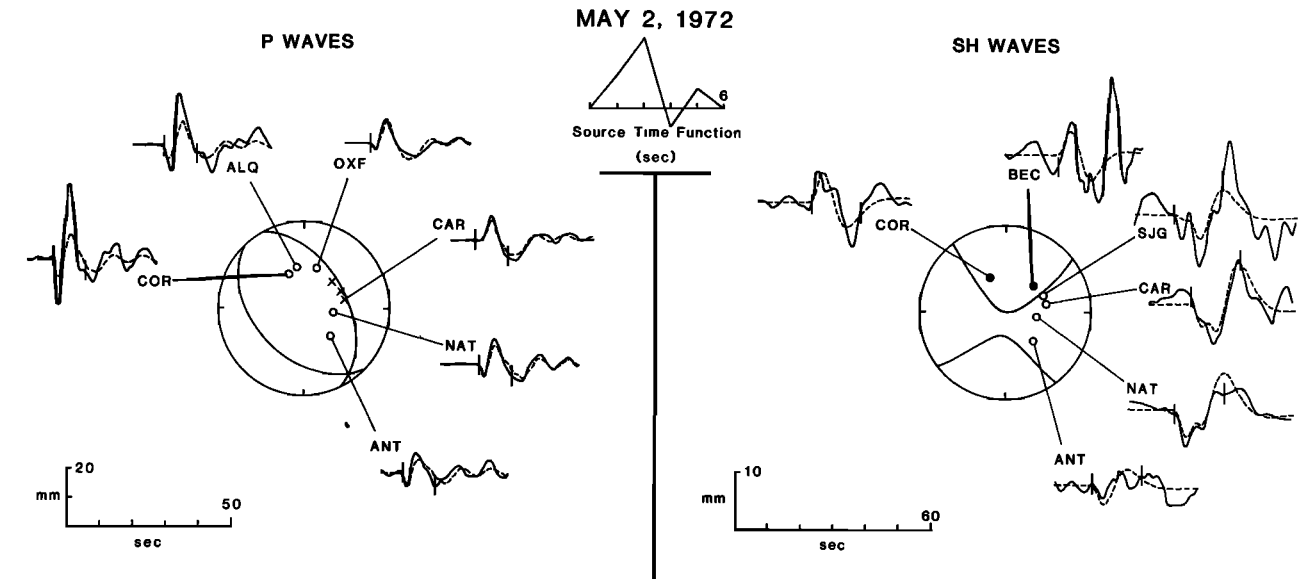


Fig. A17. Comparison of the observed and synthetic *P* and *SH* waves for the May 2, 1972, event. See Figure A2 for further explanation.

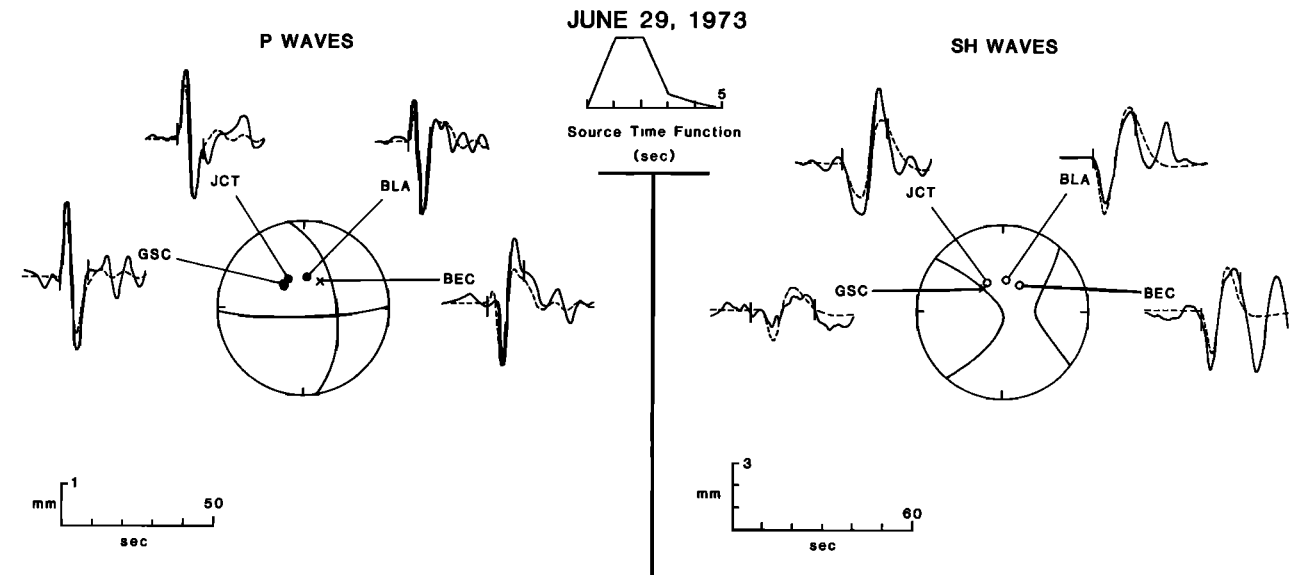


Fig. A18. Comparison of the observed and synthetic *P* and *SH* waves for the June 29, 1973, event. See Figure A2 for further explanation.

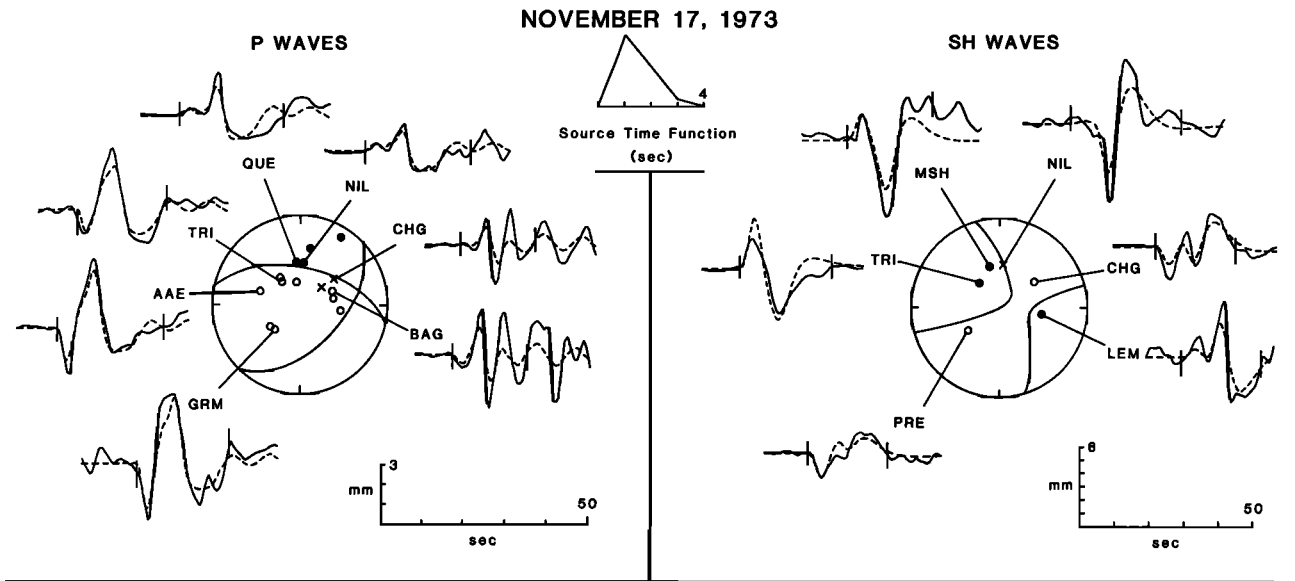


Fig. A19. Comparison of the observed and synthetic *P* and *SH* waves for the November 17, 1973, event. See Figure A2 for further explanation.

September 11, 1975 (Figures 11 and A22)

The epicenter of this earthquake is indistinguishable from that of the large event of January 21, 1970, discussed above. As with other events in the eastern Pacific, station distribution is poor. The inversion converges to a thrust-faulting mechanism (307/44/93) which is very similar to that of the 1970 event. Both original horizontal component waveforms at NNA are large and clearly recorded; the absence of either direct or reflected *SH* energy at this station provides a strong constraint on the mechanism. The *SH* waves at GSC and GOL are almost naturally rotated onto the E-W component and are clearly recorded, but the *SH* waves at several other stations, although large, appear to have been contaminated by *SV* energy and were not used in the inversion. The depth is 5 km, and the seismic moment is  $1.1 \times 10^{25}$  dyn cm.

March 29, 1976 (Figures 10 and A23)

A good match to the observed waveforms for this earthquake is obtained with a focal mechanism (199/82/181) characterized by nearly pure strike-slip motion, similar to the mechanism determined by Pennington [1981]. The mechanism is similar to that of the nearby September 9, 1965, earthquake, but the nodal planes differ in strike by about  $25^\circ$  (Figure 10). The depth is 8 km, and the seismic moment is  $9.2 \times 10^{25}$  dyn cm.

August 26, 1977 (Figures A24 and A25)

In a preliminary study of this earthquake, Creavan *et al.* [1979] reported a mechanism, based on first motion polarities and several records of long-period Rayleigh waves, characterized by nearly pure right-lateral strike-slip motion on

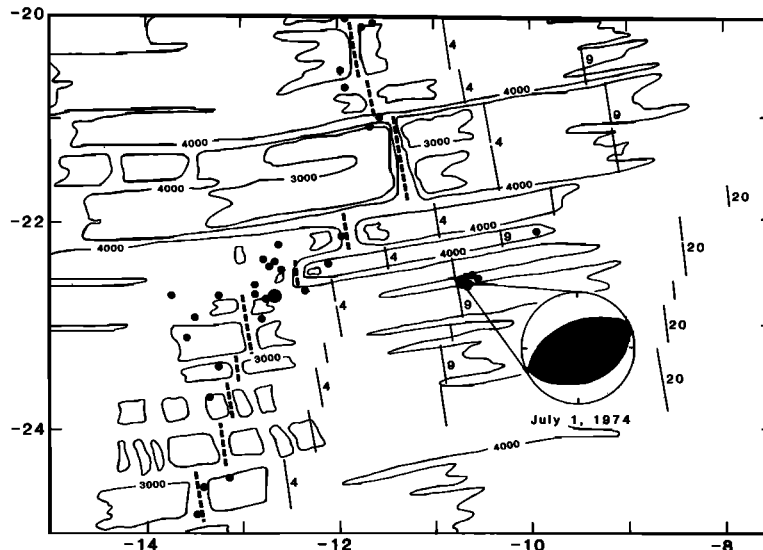


Fig. A20. Bathymetry, seismicity, and isochrons in the epicentral region of July 1, 1974, earthquake, near the South Atlantic Ridge. Bathymetric contours (3000 and 4000 m) are from Heezen and Tharp [1978]. See Figure 6 for further explanation.

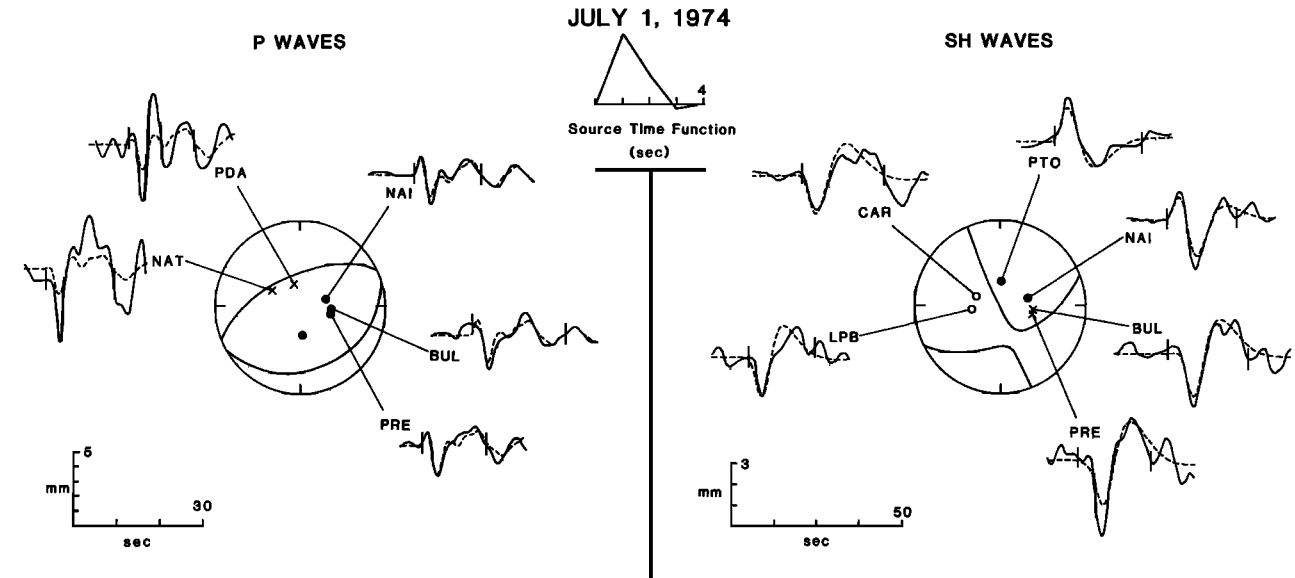


Fig. A21. Comparison of the observed and synthetic *P* and *SH* waves for the July 1, 1974, event. See Figure A2 for further explanation.

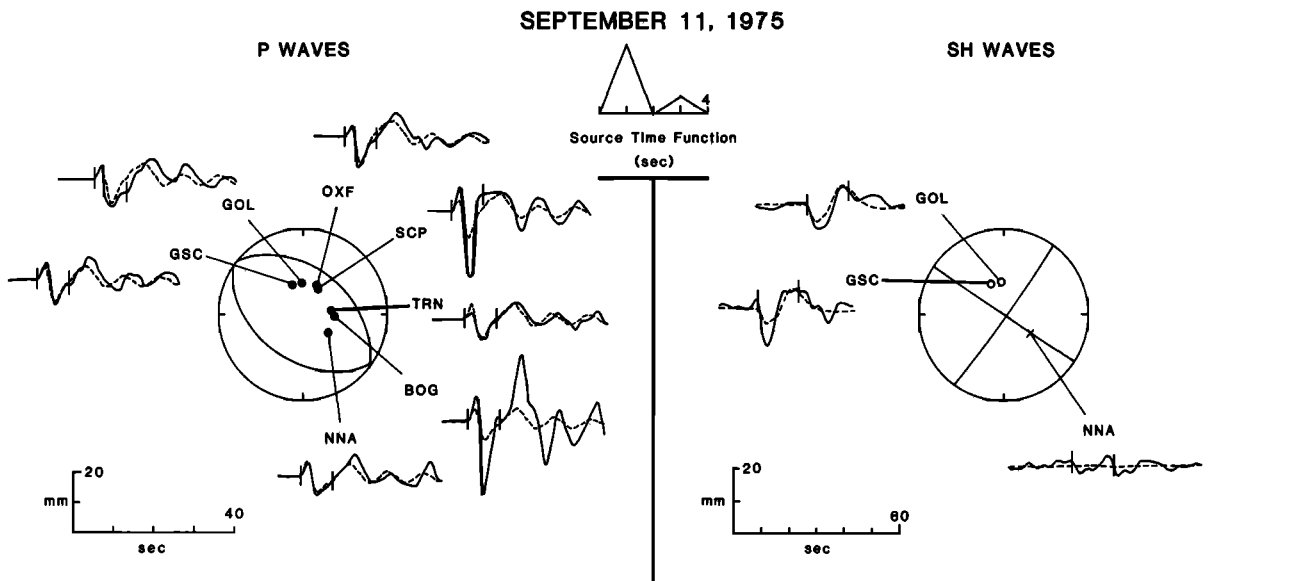


Fig. A22. Comparison of the observed and synthetic *P* and *SH* waves for the September 11, 1975, event. See Figure A2 for further explanation.

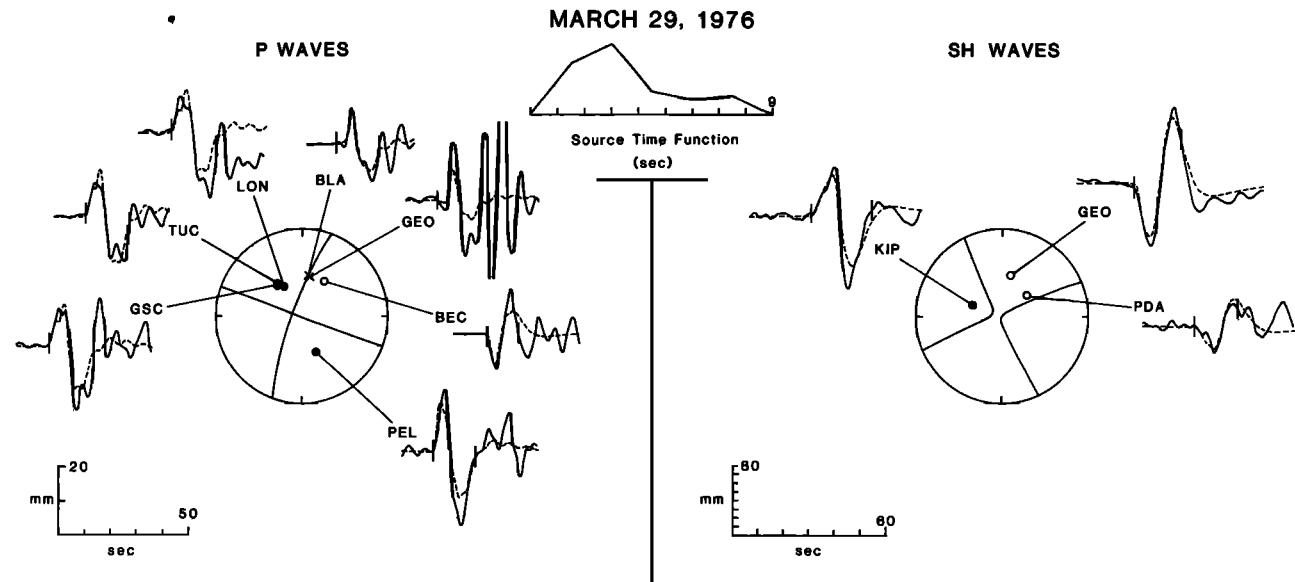


Fig. A23. Comparison of the observed and synthetic *P* and *SH* waves for the March 29, 1976, event. See Figure A2 for further explanation.

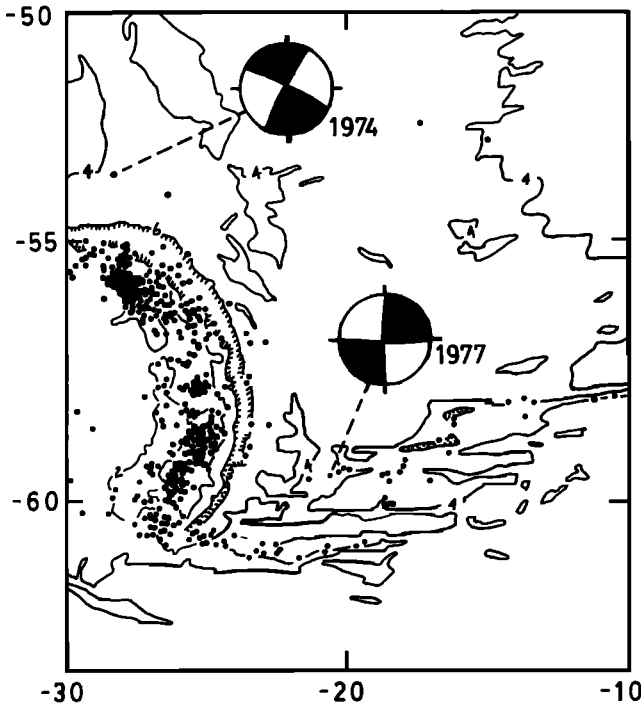


Fig. A24. Bathymetry and seismicity in the epicentral region of the August 26, 1977, earthquake, near the South Sandwich Arc. The mechanism of the November 20, 1974, intraplate earthquake, which occurred in older lithosphere than is considered in this study, is also shown. Adapted from Figure 2 of Lawver and Dick [1983]; 2-km contour interval.

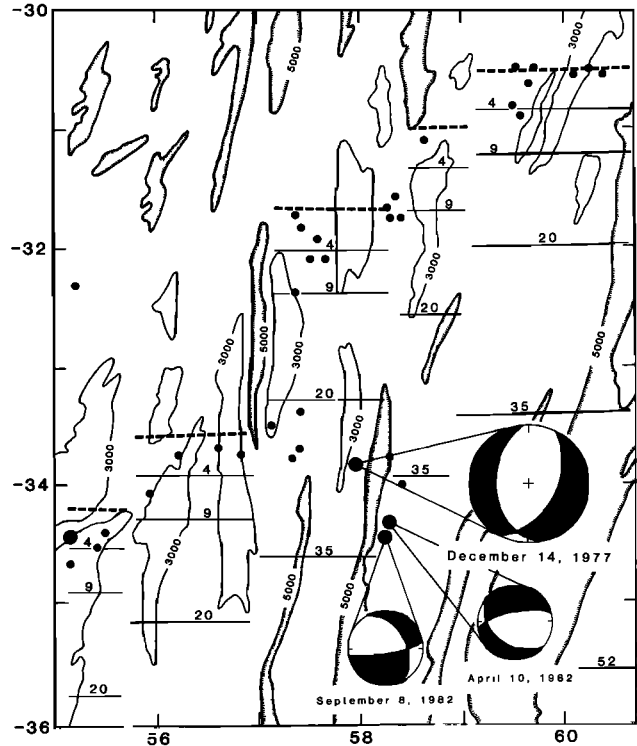


Fig. A26. Bathymetry, seismicity, and isochrons in the epicentral region of December 14, 1977, earthquake, near the Southwest Indian Ridge. Bathymetric contours (3000 and 5000 m) are from Fisher et al. [1982]. The focal mechanisms for two other earthquakes near the December 1977 event, determined by Dziewonski et al. [1983], are also shown. See Figure 6 for further explanation.

an E-W striking plane. They also estimated the seismic moment to be about  $1 \times 10^{27}$  dyn cm. We were unable to obtain any SH waveforms for this event because every shear wave record we examined was either clipped or too faint to digitize. We used P waves at six well-distributed stations, but with such a small data set we can expect to achieve only a rather crude understanding of such a large and undoubtedly complex event. The point source approximation for the long-

period body wave modeling technique is not likely to be valid for an earthquake this large. Nevertheless, we were able to achieve a reasonably good fit to the P waveforms with a simple source about 8 s in duration and a mechanism of the sort proposed by Creavan and co-workers (91/85/175). The centroid depth is 9 km, with an uncertainty of several kilometers. The seismic moment determined from the P waves is  $5.4 \times 10^{26}$  dyn cm, larger than any other event in this study. It is quite likely that the true seismic moment of this event is even larger, however, as suggested by Creavan et al. [1979].

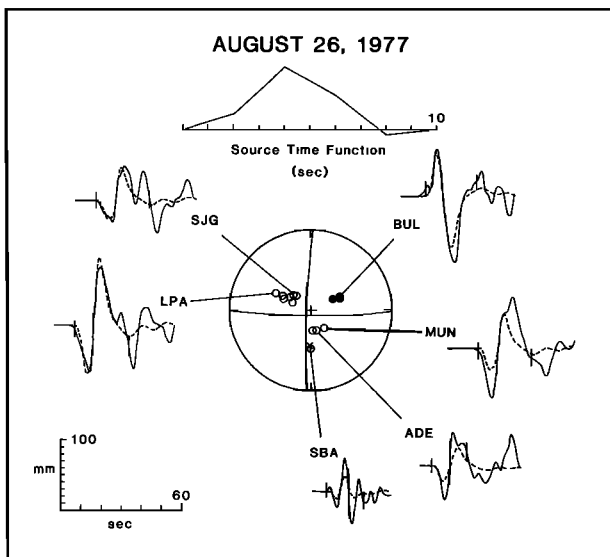


Fig. A25. Comparison of the observed and synthetic P waves for the August 26, 1977, earthquake. See Figure A2 for further explanation.

December 14, 1977 (Figures A26 and A27)

The station distribution for this event is poor, but the P waveforms clearly require a normal-faulting mechanism and the SH waveforms constrain the strike (18/51/288). The centroid depth which provides the best fit to both P and SH waves is 6 km, but the source time function is unusually long (6 s) for the seismic moment ( $2.8 \times 10^{24}$  dyn cm), implying a very low stress drop for this event. An equally good fit to the P waveforms can be obtained with a source at a centroid depth of about 17 km and a source time function 3 s long, but none of the SH waves could be satisfactorily matched with this solution. The nodal planes are subparallel to the trend of the many fracture zones in the epicentral region. Dziewonski et al. [1983] report mechanisms for two other small events (April 10, 1982, and September 8, 1982) very near this one, both with larger components of strike-slip motion than we found for the December 1977 event (Table 1).

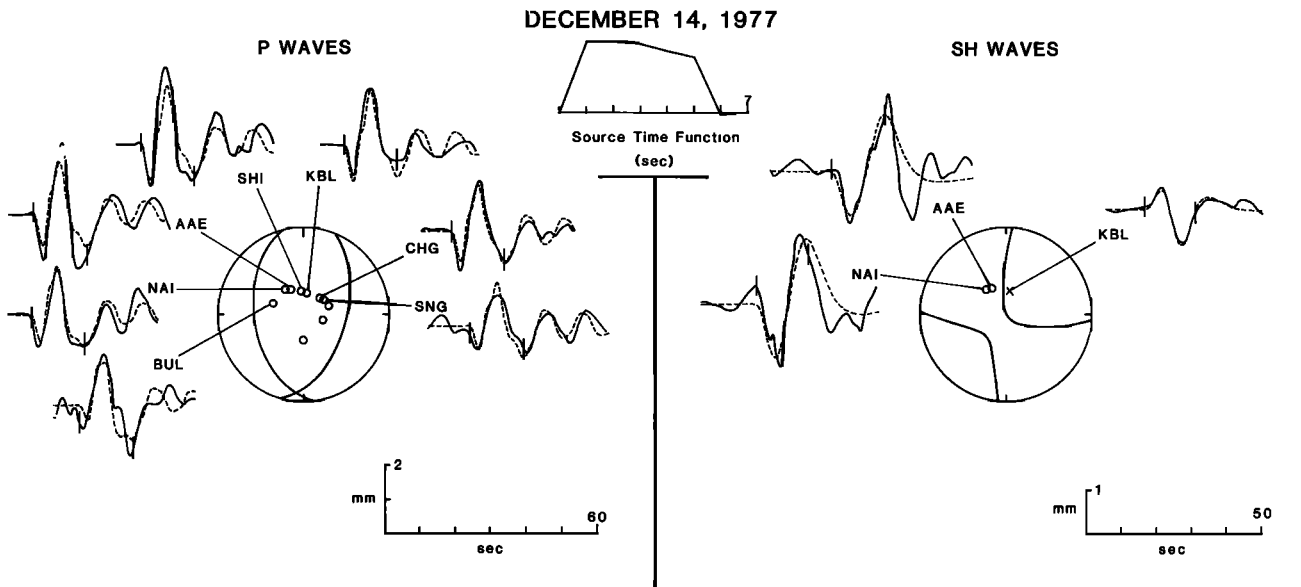


Fig. A27. Comparison of the observed and synthetic *P* and *SH* waves for the December 14, 1977, event. See Figure A2 for further explanation.

December 13, 1979 (Figures 10 and A28)

The station distribution for this event is very poor, and very few *P* waves are suitable for waveform modeling. The *SH* waves are relatively large and well recorded, however, because the mechanism is characterized by nearly pure strike-slip motion (349/75/178). The first-motion polarities which appear to be violated by the inversion mechanism may have been read from one of the surface-reflected phases rather than the direct *P* phase, which is very small at some stations (e.g., WES). The depth is 13 km, and the seismic moment is  $8.7 \times 10^{24}$  dyn cm. North striking fracture zones are found in the region, and the nodal plane striking slightly west of north is probably the fault plane for this event. The *SH* wave at PEL has a distinctly shorter period than the *SH* waves to the north. In order to reproduce this feature we modeled this event as a

horizontally propagating point source, with the rupture propagating toward the south (N169°E) at 3.2 km/s. The source time function is composed of overlapping trapezoidal elements whose apparent duration at each station depends on the angle between the rupture vector and the departing ray at the source [Nabelek, 1984].

September 13, 1981 (Figures A29 and A30)

Dziewonski and Woodhouse [1983] reported a focal mechanism (74/29/290) for this earthquake characterized by normal faulting on nodal planes striking at a high angle to the axial trend of the nearby Mid-Atlantic Ridge. This earthquake was very well recorded, and the station distribution for both *P* and *SH* waves is excellent. Our best fitting mechanism (21/33/264) is very similar to that of Dziewonski and Woodhouse [1983]

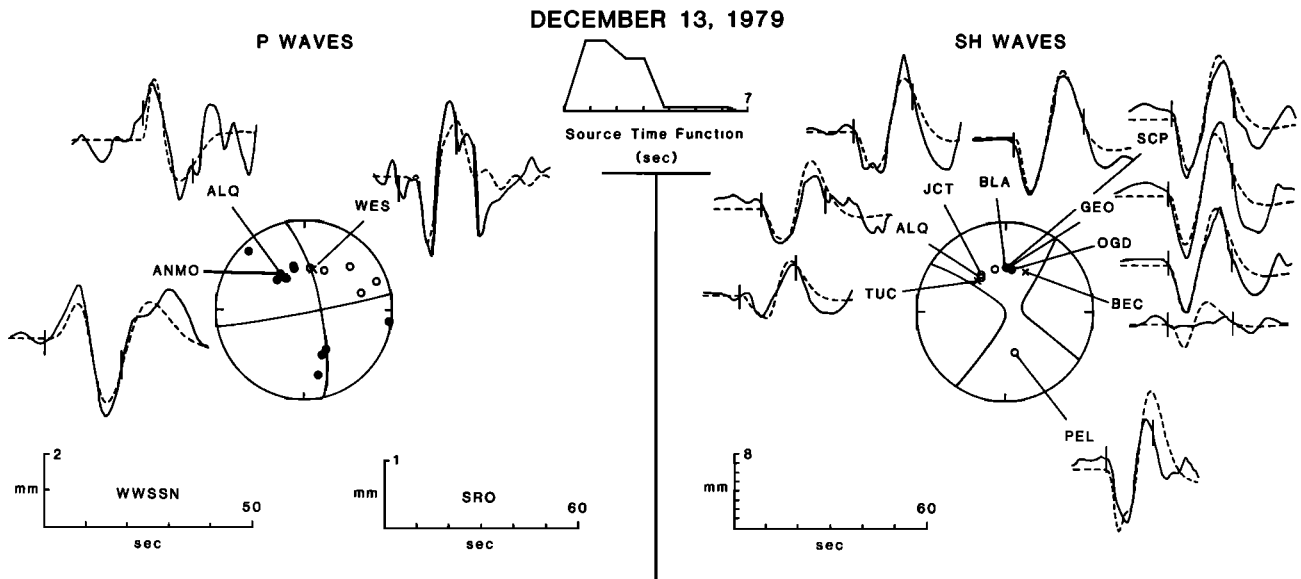


Fig. A28. Comparison of the observed and synthetic *P* and *SH* waves for the December 13, 1979, event. ANMO is a Seismic Research Observatory (SRO) station and has a separate time-amplitude scale. This event was modeled as a horizontally propagating point source, rupturing toward the south (azimuth N169°E) at 3.2 km/s. See the appendix and Figure A2 for further explanation.

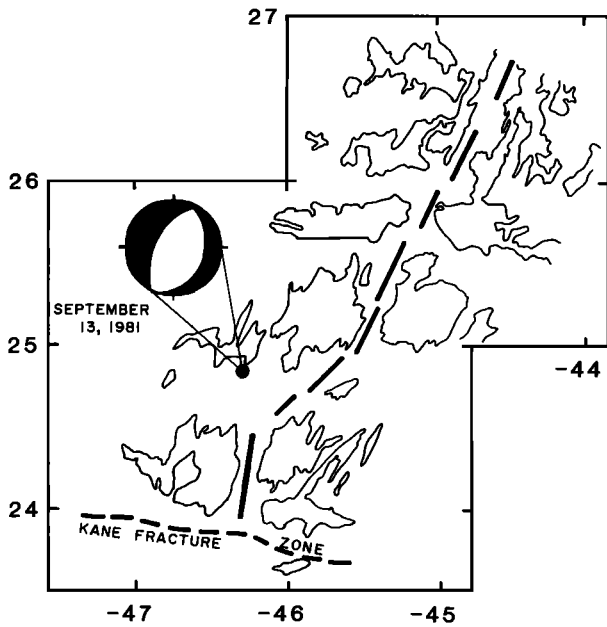


Fig. A29. Bathymetry and tectonic elements in the epicentral region of the September 13, 1981, earthquake, adapted from Figure 3 of Rona and Gray [1980]. Rift mountains are outlined by the 3000-m isobath. The positions of ridge axis segments and the Kane Fracture Zone are indicated by heavy lines.

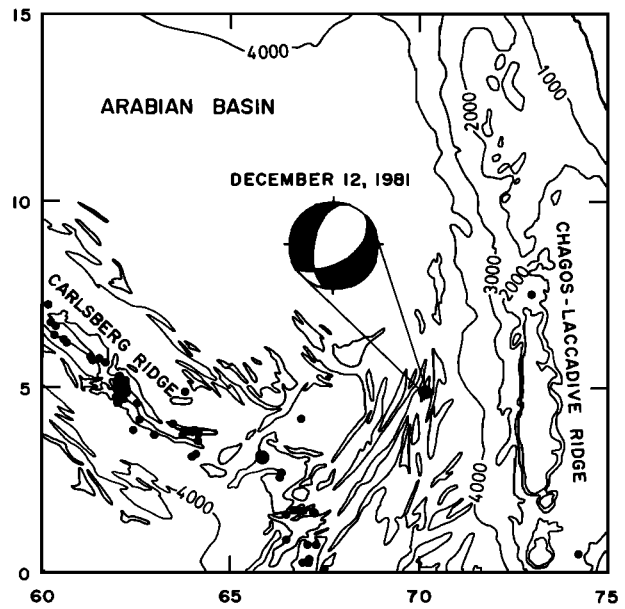


Fig. A31. Bathymetry and seismicity in the epicentral region of the December 12, 1981, earthquake. Bathymetry from Laughton [1975]; 1000-m contour interval.

except that the fault strike is rotated about 50°, bring it parallel to the trend of the ridge axis. The inversion converged to this solution even when the Dziewonski and Woodhouse mechanism was used as a starting model. The nodal SH wave at TUC is the major factor controlling the strike; the Dziewonski and Woodhouse mechanism produces a severe misfit at this station. The steeply dipping nodal plane is required to fit the P waveforms at LPS and SCP (a number of other nearby stations have similar waveforms), at which no dilatational motion is seen. The seismic moment is  $8.9 \times 10^{24}$  dyn cm, in excellent agreement with the moment of  $8.95 \times 10^{24}$

dyn cm found by Dziewonski and Woodhouse. The centroid depth is 11 km.

December 12, 1981 (Figures A31 and A32)

Because of the small size and recent date of this event, few waveforms suitable for modeling were obtained. Our P waveform data cover an azimuthal arc of only about 60°. We found three usable SH waves which cover one hemisphere. These data, while sparse, yielded a reasonably good solution (60/50/307) characterized by normal faulting on planes parallel to the local fracture zone trend. The centroid depth is 15 km, and the seismic moment is  $2.3 \times 10^{24}$  dyn cm.

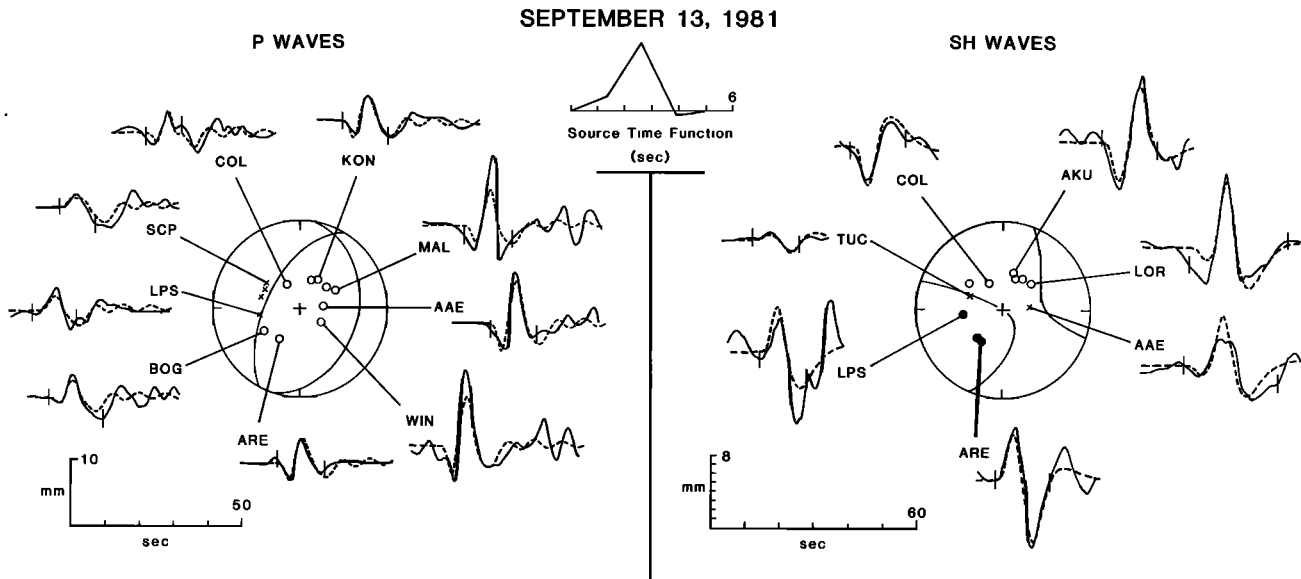


Fig. A30. Comparison of the observed and synthetic P and SH waves for the September 13, 1981, earthquake. See Figure 2 for further explanation.

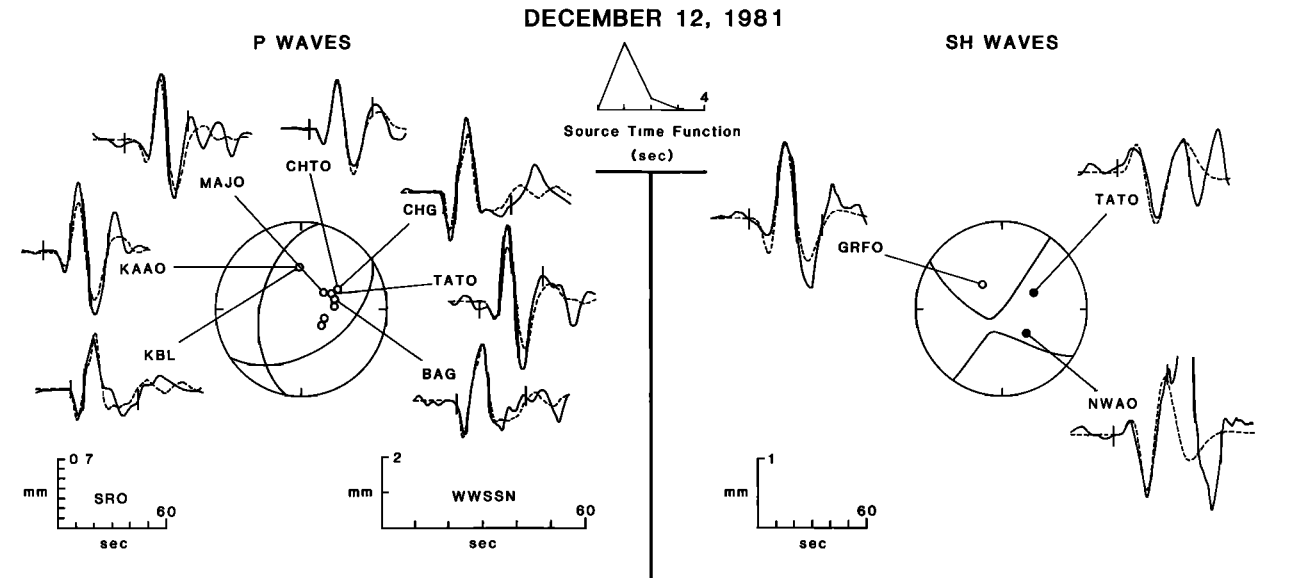


Fig. A32. Comparison of the observed and synthetic  $P$  and  $SH$  waves for the December 12, 1981, earthquake. There are separate time-amplitude scales for  $P$  waves recorded at WWSSN (KBL, CHG, and BAG) and GDSN stations (TATO, CHTO, MAJO, and KAAO). See Figure 2 for further explanation.

**Acknowledgments.** We thank John Nabelek for tutoring in the art of investigating earthquake source processes with waveform modeling, Doug Wiens and Seth Stein for stimulating conversations and friendly competition, Jeff Weissel for discussions on geoid height data and its possible relation to small-scale convection beneath young oceanic lithosphere, and Roger Buck for discussions on numerical models of variable-viscosity convection. We are grateful to James Dewey, Gordon Stewart, and Doug Wiens for constructive reviews of an earlier draft. We also thank Jan Nattier-Barbaro for help with manuscript preparation, Linda Meinke for assistance with figure preparation, and Susan Saarinen for drafting the figures. This research was supported by the National Aeronautics and Space Administration under grant NAG5-44 and contract NAS 5-27339, by the National Science Foundation under grant EAR-8115908, and by a fellowship (S.C.S) from the John Simon Guggenheim Memorial Foundation.

#### REFERENCES

- Aki, K., and P. G. Richards, *Quantitative Seismology: Theory and Methods*, vol. 1, p. 114, W. H. Freeman, San Francisco, Calif., 1980.
- Anderson, R. N., D. W. Forsyth, P. Molnar, and J. Mammertx, Fault plane solutions of earthquakes on the Nazca plate boundaries and the Easter plate, *Earth Planet. Sci. Lett.*, **24**, 188-202, 1974.
- Artyushkov, E. V., Stresses in the lithosphere caused by crustal thickness inhomogeneities, *J. Geophys. Res.*, **78**, 7675-7708, 1973.
- Banghar, A. R., and L. R. Sykes, Focal mechanisms of earthquakes in the Indian Ocean and adjacent regions, *J. Geophys. Res.*, **74**, 632-649, 1969.
- Bergman, E. A., Intraplate earthquakes and the state of stress in oceanic lithosphere, Ph.D. thesis, 448 pp., Mass. Inst. of Technol., Cambridge, 1984.
- Bergman, E. A., and S. C. Solomon, Oceanic intraplate earthquakes: Implications for local and regional intraplate stress, *J. Geophys. Res.*, **85**, 5389-5410, 1980.
- Bergman, E. A., and S. C. Solomon, Source studies of near-ridge earthquakes: Implications for the early evolution of oceanic lithosphere (abstract), *Eos Trans. AGU*, **64**, 759, 1983.
- Bergman, E. A., J. L. Nabelek, and S. C. Solomon, An extensive region of off-ridge normal-faulting earthquakes in the southern Indian Ocean, *J. Geophys. Res.*, **89**, 2425-2443, 1984.
- Brace, W. F., and D. L. Kohlstedt, Limits on lithospheric stress imposed by laboratory experiments, *J. Geophys. Res.*, **85**, 6248-6252, 1980.
- Buck, W. R., Small-scale convection and the evolution of the lithosphere, Ph.D. thesis, 257 pp., Mass. Inst. of Technol., Cambridge, 1984.
- Byerlee, J. D., Friction of rocks, *Pure Appl. Geophys.*, **116**, 615-626, 1978.
- Caristan, Y., The transition from high-temperature creep to fracture in Maryland diabase, *J. Geophys. Res.*, **87**, 6781-6790, 1982.
- Carlsaw, H. S., and J. D. Jaeger, *Conduction of Heat in Solids*, 2nd ed., 510 pp., Oxford University Press, New York, 1959.
- Chapple, W. M., and D. W. Forsyth, Earthquakes and bending of plates at trenches, *J. Geophys. Res.*, **84**, 6729-6749, 1979.
- Chen, W.-P., and P. Molnar, Focal depths of intracontinental and intraplate earthquakes and their implications for the thermal and mechanical properties of the lithosphere, *J. Geophys. Res.*, **88**, 4183-4214, 1983.
- Chinnery, M. A., Measurement of  $m_b$  with a global network, *Tectonophysics*, **49**, 139-144, 1978.
- Creavan, C. T., H. Kanamori, and K. Fujita, A large intraplate event near the Scotia Arc (abstract), *Eos Trans. AGU*, **60**, 894, 1979.
- Dahlen, F. A., Isostasy and the ambient state of stress in the oceanic lithosphere, *J. Geophys. Res.*, **86**, 7801-7807, 1981.
- Drummond, K. J., Plate tectonic map of the Circum-Pacific region, northeast quadrant, Am. Assoc. of Pet. Geol., Tulsa, Okla., 1981.
- Dziewonski, A. M., and J. H. Woodhouse, An experiment in systematic study of global seismicity: Centroid-moment tensor solutions for 201 moderate and large earthquakes of 1981, *J. Geophys. Res.*, **88**, 3247-3272, 1983.
- Dziewonski, A. M., A. Friedman, D. Giardini, and J. H. Woodhouse, Global seismicity of 1982: Centroid-moment tensor solutions for 308 earthquakes, *Phys. Earth Planet. Inter.*, **33**, 76-90, 1983.
- Epp, D., and W. Suyenaga, Thermal contraction and alteration of the oceanic crust, *Geology*, **6**, 726-728, 1978.
- Ewing, J. I., and R. Houtz, Acoustic stratigraphy and structure of the oceanic crust, in *Deep Drilling Results in the Atlantic Ocean: Ocean Crust, Maurice Ewing Ser.*, vol. 2, edited by M. Talwani, C. G. Harrison, and D. E. Hayes, pp. 1-14, AGU, Washington, D. C., 1979.
- Falconer, R. H. K., and M. Tharp, General bathymetric chart of the oceans (GEBCO), 5th ed., sheet 5.14, Can. Hydrogr. Serv., Ottawa, 1981.
- Fehn, U., and L. M. Cathles, Hydrothermal convection at slow-spreading mid-ocean ridges, *Tectonophysics*, **55**, 239-260, 1979.
- Fisher, R. L., M. Z. Jantsch, and R. L. Comer, General bathymetric chart of the oceans (GEBCO), 5th ed., sheet 5.09, Can. Hydrogr. Serv., Ottawa, 1982.
- Fleitout, L., and C. Froidevaux, Tectonic stresses in the lithosphere, *Tectonics*, **2**, 315-324, 1983.
- Forsyth, D. W., Compressive stress between two mid-ocean ridges, *Nature*, **243**, 78-79, 1973.
- Forsyth, D. W., Fault plane solutions and tectonics of the South Atlantic and Scotia Sea, *J. Geophys. Res.*, **80**, 1429-1443, 1975.
- Goetze, C., and B. Evans, Stress and temperature in the bending lithosphere as constrained by experimental rock mechanics, *Geophys. J. R. Astron. Soc.*, **59**, 463-478, 1979.

- Haxby, W. F., and J. K. Weissel, Evidence for small-scale mantle convection from Seasat altimeter data (abstract), *Eos Trans. AGU*, 64, 838, 1983.
- Hayes, D. E., and M. Vogel, General bathymetric chart of the oceans (GEBCO), 5th ed., sheet 5.13, Can. Hydrogr. Serv., Ottawa, 1981.
- Heezen, B. C., and M. Tharp, General bathymetric chart of the oceans (GEBCO), 5th ed., sheet 5.12, Can. Hydrogr. Serv., Ottawa, 1978.
- Huang, P. Y., S. C. Solomon, E. A. Bergman, and J. L. Nabelek, Focal depths and mechanisms of Mid-Atlantic Ridge earthquakes from body waveform inversion (abstract), *Eos Trans. AGU*, 65, 2732, 1984.
- Jemsek, J. P., E. A. Bergman, J. L. Nabelek, and S. C. Solomon, Focal depths and mechanisms of large earthquakes on the Mid-Arctic Ridge system (abstract), *Eos Trans. AGU*, 65, 273, 1984.
- Kirby, S. H., Tectonic stresses in the lithosphere, constraints provided by the experimental deformation of rocks, *J. Geophys. Res.*, 85, 6353-6363, 1980.
- LaBrecque, J. L., and P. D. Rabinowitz, General bathymetric chart of the oceans (GEBCO), 5th ed., sheet 5.16, Can. Hydrogr. Serv., Ottawa, 1981.
- LaBrecque, J. L., D. V. Kent, and S. C. Cande, Revised magnetic polarity time scale for Late Cretaceous and Cenozoic time, *Geology*, 5, 330-335, 1977.
- Laughton, A. S., General bathymetric chart of the oceans (GEBCO), 5th ed., sheet 5.05, Can. Hydrogr. Serv., Ottawa, 1975.
- Lawver, L. A., and H. J. B. Dick, The American-Antarctic Ridge, *J. Geophys. Res.*, 88, 8193-8202, 1983.
- Lister, C. R. B., Gravitational drive on oceanic plates caused by thermal contraction, *Nature*, 257, 663-665, 1975.
- Lister, C. R. B., Qualitative models of spreading-center processes, including hydrothermal penetration, *Tectonophysics*, 37, 203-218, 1977.
- Macdonald, K. C., and T. M. Atwater, Evolution of rifted ocean ridges, *Earth Planet. Sci. Lett.*, 39, 319-327, 1978.
- Mammerickx, J., and S. M. Smith, General bathymetric chart of the oceans (GEBCO), 5th ed., sheet 5.11, Can. Hydrogr. Serv., Ottawa, 1980.
- Mammerickx, J., and S. M. Smith, General bathymetric chart of the oceans (GEBCO), 5th ed., sheet 5.07, Can. Hydrogr. Serv., Ottawa, 1982.
- Meissner, R., and J. Strehlau, Limits of stresses in continental crusts and their relation to the depth-frequency distribution of shallow earthquakes, *Tectonics*, 1, 73-90, 1982.
- Mendiguren, J. A., Focal mechanism of a shock in the middle of the Nazca plate, *J. Geophys. Res.*, 76, 3861-3879, 1971.
- Minster, J. B., and T. H. Jordan, Present-day plate motions, *J. Geophys. Res.*, 83, 5331-5354, 1978.
- Molnar, P., and L. R. Sykes, Tectonics of the Caribbean and Middle America regions from focal mechanisms and seismicity, *Geol. Soc. Am. Bull.*, 80, 1639-1684, 1969.
- Morgan, W. J., Rodriguez, Darwin, Amsterdam, . . . , A second type of hot spot island, *J. Geophys. Res.*, 83, 5355-5360, 1978.
- Nabelek, J. L., Determination of earthquake source parameters from inversion of body waves, Ph.D. thesis, 346 pp., Mass. Inst. of Technol., Cambridge, 1984.
- Parsons, B., and D. McKenzie, Mantle convection and the thermal structure of the plates, *J. Geophys. Res.*, 83, 4485-4496, 1978.
- Parsons, B., and J. G. Sclater, An analysis of the variation of ocean floor bathymetry and heat flow with age, *J. Geophys. Res.*, 82, 803-827, 1977.
- Pennington, W. D., Subduction of the eastern Panama Basin and seismotectonics of northwestern South America, *J. Geophys. Res.*, 86, 10753-10770, 1981.
- Piffner, O. A., and J. G. Ramsay, Constraints on geological strain rates: Arguments from finite strain states of naturally deformed rocks, *J. Geophys. Res.*, 87, 311-321, 1982.
- Poppe, B. B., D. A. Naab, and J. S. Perry, Seismograph station codes and characteristics, *U.S. Geol. Surv. Circ.*, 791, 171 pp., 1978.
- Richardson, R. M., S. C. Solomon, and N. H. Sleep, Tectonic stress in the plates, *Rev. Geophys. Space Phys.*, 17, 981-1019, 1979.
- Richter, F. M., Convection and large-scale circulation of the mantle, *J. Geophys. Res.*, 78, 8735-8745, 1973.
- Richter, F. M., and B. Parsons, On the interaction of two scales of convection in the mantle, *J. Geophys. Res.*, 80, 2529-2541, 1975.
- Rona, P. A., and D. F. Gray, Structural behavior of fracture zones symmetric and asymmetric about a spreading axis: Mid-Atlantic Ridge (latitude 23°N to 27°N), *Geol. Soc. Am. Bull.*, 91, 485-494, 1980.
- Schlich, R., The Indian Ocean: Aseismic ridges, spreading centers, and ocean basins, in *The Ocean Basins and Margins*, vol. 6: *The Indian Ocean*, edited by A. E. M. Nairn and F. G. Stehli, pp. 51-148, Plenum, New York, 1982.
- Schouten, H., and R. S. White, Zero offset fracture zones, *Geology*, 8, 175-179, 1980.
- Sclater, J. G., C. Jaupart, and D. Galson, The heat flow through oceanic and continental crust and the heat loss of the earth, *Rev. Geophys. Space Phys.*, 18, 269-311, 1980.
- Searle, R. C., D. Monahan, and G. L. Johnson, General bathymetric chart of the oceans (GEBCO), 5th ed., sheet 5.08, Can. Hydrogr. Serv., Ottawa, 1982.
- Solomon, S. C., E. A. Bergman, and P. Y. Huang, Earthquakes and tectonics at mid-ocean ridge axes (abstract), *Eos Trans. AGU*, 64, 759, 1983.
- Stein, S., An earthquake swarm on the Chagos-Laccadive Ridge and its tectonic implications, *Geophys. J. R. Astron. Soc.*, 55, 577-588, 1978.
- Stein, S., and D. A. Wiens, Implications of oceanic intraplate seismicity for intraplate stresses, plate driving forces and mantle viscosity (abstract), *Eos Trans. AGU*, 64, 759, 1983.
- Sykes, L. R., Mechanism of earthquakes and nature of faulting on the mid-oceanic ridges, *J. Geophys. Res.*, 72, 2131-2153, 1967.
- Sykes, L. R., Earthquake swarms and sea-floor spreading, *J. Geophys. Res.*, 75, 6598-6611, 1970a.
- Sykes, L. R., Seismicity of the Indian Ocean and a possible nascent island arc between Ceylon and Australia, *J. Geophys. Res.*, 75, 5041-5055, 1970b.
- Sykes, L. R., Intraplate seismicity, reactivation of preexisting zones of weakness, alkaline magmatism, and other tectonism postdating continental fragmentation, *Rev. Geophys. Space Phys.*, 16, 621-688, 1978.
- Sykes, L. R., and M. L. Sbar, Focal mechanism solution of intraplate earthquakes and stresses in the lithosphere, in *Geodynamics of Iceland and the North Atlantic Area*, edited by L. Kristjansson, pp. 207-224, D. Reidel, Hingham, Mass., 1974.
- Tapponnier, P., and J. Francheteau, Necking of the lithosphere and the mechanics of slowly accreting plate boundaries, *J. Geophys. Res.*, 83, 3955-3970, 1978.
- Tarantola, A., and B. Valette, Generalized nonlinear inverse problems solved using the least squares criterion, *Rev. Geophys. Space Phys.*, 20, 219-232, 1982.
- Tobin, D. G., and L. R. Sykes, Seismicity and tectonics of the northeast Pacific Ocean, *J. Geophys. Res.*, 73, 3821-3845, 1968.
- Tréhu, A. M., J. L. Nábělek, and S. C. Solomon, Source characterization of two Reykjanes Ridge earthquakes: Surface waves and moment tensors; *P* waveforms and nonorthogonal nodal planes, *J. Geophys. Res.*, 86, 1701-1734, 1981.
- Turcotte, D. L., Are transform faults thermal contraction cracks?, *J. Geophys. Res.*, 79, 2573-2577, 1974.
- Turcotte, D. L., and E. R. Oxburgh, Mid-plate tectonics *Nature*, 244, 337-339, 1973.
- Wang, S.-C., R. J. Geller, S. Stein, and B. Taylor, An intraplate thrust faulting earthquake in the South China Sea, *J. Geophys. Res.*, 84, 5627-5631, 1979.
- Watts, A. B., J. H. Bodine, and M. S. Steckler, Observations of flexure and the state of stress in the oceanic lithosphere, *J. Geophys. Res.*, 85, 6369-6376, 1980.
- Wiens, D. A., and S. Stein, Age dependence of oceanic intraplate seismicity and implications for lithospheric evolution, *J. Geophys. Res.*, 88, 6455-6468, 1983a.
- Wiens, D. A., and S. Stein, Near ridge intraplate stress heterogeneities inferred from earthquake mechanisms (abstract), *Eos Trans. AGU*, 64, 269, 1983b.
- Wiens, D. A., and S. Stein, Implications of oceanic intraplate seismicity for plate stresses, driving forces and rheology, *Tectonophysics*, in press, 1984.
- Wiens, D. A., C. M. Helm, and S. Stein, Intraplate seismicity and stresses in young oceanic lithosphere (abstract), *Eos Trans. AGU*, 64, 759, 1983.

E. A. Bergman and S. C. Solomon, Department of Earth, Atmospheric, and Planetary Sciences, Massachusetts Institute of Technology, 54-512, Cambridge, MA 02139.

(Received January 23, 1984;  
revised September 7, 1984;  
accepted September 11, 1984.)